Hydrogen Abstraction by Chlorine Atom from Small Organic Molecules Containing Amino Acid Functionalities: An Assessment of Theoretical Procedures†

Mark S. Taylor,*,‡,§ Sandra A. Ivanic,‡,§ Geoffrey P. F. Wood,‡,§ Christopher J. Easton,§,|| George B. Bacskay,‡ and Leo Radom*,‡,§

ARC Centre of Excellence for Free Radical Chemistry and Biotechnology, School of Chemistry, University of Sydney, Sydney, NSW 2006, Australia, and Research School of Chemistry, Australian National University, Canberra, ACT 0200, Australia

Received: March 31, 2009; Revised Manuscript Received: May 22, 2009

A high-level quantum chemistry investigation has been carried out for the abstraction by chlorine atom of hydrogen from methane and five monosubstituted methanes, chosen to reflect the chemical functionalities contained in amino acids and peptides. A modified W1′ procedure is used to calculate benchmark barriers and reaction energies for the six reactions. The reactions demonstrate a broad range of barrier heights and reaction energies, which can be rationalized using curve-crossing and molecular orbital theory models. In addition, the performance of a range of computationally less demanding electronic structure methods is assessed for calculating the energy profiles for the six reactions. It is found that the G3X(MP2)-RAD procedure compares best with the W1′ benchmark, demonstrating a mean absolute deviation (MAD) from W1′ of 2.1 kJ mol^{-1}. The more economical RMP2/G3XLarge and UB2-PLYP/G3XLarge methods are also shown to perform well, with MADs from W1′ of 2.9 and 3.0 kJ mol^{-1}, respectively.

1. Introduction

The series of reactions in which a chlorine atom abstracts a hydrogen atom from an organic molecule is important in atmospheric and combustion chemistry and has provided models for studies of reaction dynamics and kinetics in the gas and condensed phases. In the stratosphere, H-atom abstraction from volatile organic compounds (VOC) provides a sink for the ozone-destroying Cl atom,[1] while in the troposphere, similar reactions paradoxically provide a significant source of ozone and other photochemical pollutants in coastal and industrialized regions.[2] Recent experimental studies have suggested that abstraction of H atoms from organic molecules by Cl atoms during the combustion of chlorinated materials promotes the formation of environmental pollutants such as dioxins and polychlorinated biphenyls (PCBs).[3] An extensive set of experimental studies has examined the kinetics and dynamics of several of these reactions.[4] Hydrogen abstraction from organic molecules has also been utilized in synthetic organic chemistry to functionalize molecules and to facilitate synthetic transformations.[5] In biological systems, hydrogen abstraction from biomolecules such as peptides or nucleic acids introduces a radical center into the substrate, whose subsequent reactivity may either be integral to normal cellular function[6] or lead to cellular damage and disease pathogenesis.[7]

Easton and co-workers have recently examined the photochemical chlorination of a set of amino acid and peptide related systems to determine their reactivity toward H-atom abstraction and to develop new procedures for their functionalization.[8] A subset of these experiments focused on the H-abstraction of protonated amino acids with alkyl side chains. On the basis of product distributions of chlorination, their findings revealed that the relative rates of H-atom abstraction from the side chain increase with increasing distance from the amino acid functionality. These observations were attributed to the destabilization of the polar transition structure (TS) for H-atom abstraction by inductive and polar effects associated with the NH_3^+ and CO_2H groups, thus favoring H-atom abstraction at distal sites.[8] High-level quantum chemistry calculations can potentially offer an increased understanding of these important reactions. Because most systems studied experimentally are too large for current state-of-the-art computations, it is important to assess the performance of a range of electronic structure methods on smaller model systems so as to benchmark these against the highest level of theory, which in this work is W1′.[9−12] This will provide guidance as to the choice of methods that are more readily applicable to the larger molecules of interest. Accordingly, in this work, we investigate the H-abstraction reactions of Cl atoms with six representative organic molecules (reactions 1−6) and assess the performance of a range of contemporary electronic structure methods for such calculations:

$$^{\bullet}Cl + CH_4 \rightarrow ClH + {}^{\bullet}CH_3 \quad (1)$$

$$^{\bullet}Cl + CH_3NH_3^+ \rightarrow ClH + {}^{\bullet}CH_2NH_3^+ \quad (2)$$

$$^{\bullet}Cl + CH_3CHO \rightarrow ClH + {}^{\bullet}CH_2CHO \quad (3)$$

$$^{\bullet}Cl + CH_3CO_2H \rightarrow ClH + {}^{\bullet}CH_2CO_2H \quad (4)$$

$$^{\bullet}Cl + CH_3CO_2^- \rightarrow ClH + {}^{\bullet}CH_2CO_2^- \quad (5)$$

$$^{\bullet}Cl + CH_3NH_2 \rightarrow ClH + {}^{\bullet}CH_2NH_2 \quad (6)$$

The substrate molecules in these reactions have been chosen to reflect the chemical functionalities contained in amino acids and

† Part of the "Walter Thiel Festschrift".

* To whom correspondence should be addressed. E-mail: taylor_m@chem.usyd.edu.au (M.S.T.) and radom@chem.usyd.edu.au (L.R.).

‡ University of Sydney.

§ ARC Centre of Excellence for Free Radical Chemistry and Biotechnology.

|| Australian National University.

10.1021/jp9029437 CCC: $40.75
Published on Web 07/10/2009

peptides. They are also relevant to atmospheric and combustion chemistry and fundamental chemical reaction dynamics. Several of these reactions have previously been the subject of quantum chemical investigation by other groups, and their results will be discussed in the context of the present investigation.

The structure of the present paper reflects the two broad aims of the study. First, the potential energy surfaces (PESs) for the six H-abstraction reactions, computed at the W1′ level of theory,[9−12] are examined and compared. Next, we use the W1′ results as a benchmark against which to assess the performance of computationally less-demanding theoretical procedures. As the $^{\bullet}Cl + CH_4$ reaction is the smallest and most thoroughly characterized of the six, a broader range of methods for geometry optimization and the calculation of reaction barriers and reaction energies are assessed using this prototypical reaction. Having established reliable methods for $^{\bullet}Cl + CH_4$, we then present and discuss the performance of these methods for the remaining reactions.

2. Computational Methods

Standard ab initio molecular orbital theory[13,14] and density functional theory (DFT)[14,15] calculations were performed using the GAUSSIAN 03,[16] MOLPRO 2002.6,[17] MOLPRO 2006.1,[18] and ACES II 2.5.0[19] program packages. Calculations on open-shell species employing an unrestricted wave function are designated with a "U" prefix, while calculations employing a restricted-open-shell wave function are designated with an "R" prefix. The frozen-core approximation was used in all correlated calculations, except in cases where full electron correlation was required as part of a standard composite method.

Geometries of stationary points were optimized in conjunction with the UHF, RHF, UB3-LYP, UBMK, UMP2, UQCISD, UCCSD, and UCCSD(T) methods and a range of one-electron basis sets. Following each geometry optimization, harmonic frequency analysis at the same level of theory was carried out to confirm the nature of the stationary point as a minimum (equilibrium structure) or first-order saddle point (TS). In most cases, relative energies reported in the paper are vibrationless values (designated ΔE or $\Delta E^{\ddagger}$), but in specific instances, the energies (designated ΔH or $\Delta H^{\ddagger}$) include appropriately scaled[20] harmonic zero-point vibrational energies. To fully characterize the PES of each of the six reactions, reactant and product complexes were also located.

Benchmark energies were calculated using the W1′ procedure,[9] a member of the W*n* family of methods, which collectively demonstrate excellent (on average sub-kJ mol^{-1}) agreement with experimental thermochemical properties.[9−12,21,22] The W1′ procedure approximates the exact relativistic, fixed-nuclei, basis-set-limit URCCSD(T) energy using extrapolation and additivity approximations. The scalar-relativistic correction was calculated as the expectation value of the first-order Darwin and mass-velocity terms[23] using the averaged coupled pair functional (ACPF) procedure.[24] We have used a modified W1′ procedure that employs a two-point extrapolation for each of the SCF, CCSD, and (T) energy components and excludes the chlorine 1s orbital from the core-correlation as well as the scalar-relativistic calculations.[11] Unless otherwise specified, W1′ single-point energies were calculated using geometries optimized at the UQCISD/6-31+G(d,p) level, instead of the prescribed UB3-LYP/VTZ+1 level.[10] UQCISD/6-31+G(d,p)-optimized geometries in the form of Gaussian archive files, as well as W1′ total energies, are presented for all relevant equilibrium and TSs in the Supporting Information.

The ^2P Cl atom possesses two fine-structure levels, $^2P_{3/2}$ and $^2P_{1/2}$, due to a splitting by a spin−orbit (SO) interaction of 882 cm^{-1} (10.55 kJ mol^{-1}).[25] This interaction effectively stabilizes the ground $^{\bullet}Cl$ $^2P_{3/2}$ state by 3.52 kJ mol^{-1} with respect to the nonrelativistic $^{\bullet}Cl$ ^2P energy. We have assumed that this interaction stabilizes the isolated $^2P_{3/2}$ Cl atom as well as the various $^2P_{3/2}$ $^{\bullet}Cl$-molecular complexes, while being fully quenched at all other points on the PES, such as TSs. Thus, unless stated otherwise, the electronic energies of the isolated $^2P_{3/2}$ Cl atom and all of the $^2P_{3/2}$ $^{\bullet}Cl$-molecular complexes were corrected by an invariant −3.52 kJ mol^{-1} SO term, across all levels of theory.

Two additional calculations were used to examine other aspects of the TSs. The natural bond orbital (NBO) method[26] was used to analyze the TS charge distributions, based on CCSD/6-311+G(2df,p) electron densities, calculated using UQCISD/6-31+G(d,p) geometries. To appraise the importance of charge-transfer configurations to the electronic ground states of the TSs, we calculated the relative energy of the charge-transfer Cl^- $^{\bullet}H$ R^+ configurations with respect to the covalent $^{\bullet}Cl$ $^{\bullet}H$ $^{\bullet}R$ configurations. The energy difference between the charge-transfer and covalent configurations was approximated as the difference in vertical ionization energy (IE) of isolated, optimized $^{\bullet}R$ and the electron affinity (EA) of $^{\bullet}Cl$, that is, IE($^{\bullet}R$) − EA($^{\bullet}Cl$),[27] calculated using the G3X(MP2)-RAD method,[28] at UQCISD/6-31+G(d,p)-optimized geometries.

The assessment of the performance of the various levels of theory that are computationally less demanding than W1′ employed a 2-fold approach. First, to identify appropriate levels of theory for geometry optimizations, reaction barriers and energies were calculated using UCCSD(T)/6-311+G(3df,2p) single-point energies at geometries optimized using a range of methods. Second, using UQCISD/6-31+G(d,p) geometries for all six reactions, the performance of a range of methods in calculating barriers and reaction energies was assessed. The G3X(MP2)-RAD composite procedure[28] and the double-hybrid B2-PLYP[29] DFT procedure were two of the methods used to calculate barriers and reaction energies. For both parts of the assessment study, a wider range of methods was examined for the $^{\bullet}Cl + CH_4 \rightarrow ClH + {}^{\bullet}CH_3$ reaction, and a smaller subset of these was assessed for the remaining five reactions. The largest basis sets used for the noncomposite methods for all of the reactions are 6-311+G(3df,2p) and G3XLarge.[30] The latter provides a better description of chlorine, with 3d2f1g polarization functions rather than 3d1f.

Intrinsic reaction coordinate (IRC) calculations, as implemented in Gaussian 03, were used as a basis for IRCMax evaluations of reaction barriers.[31] Following the lower-level optimization of a TS, the IRC was calculated over a small range, using the same electronic structure method. Higher-level single-point energies were next calculated along this IRC, which yielded the IRCMax point as the highest energy structure along this truncated segment of the reaction path. Petersson and co-workers have demonstrated that the IRCMax barrier is an excellent approximation to the barrier obtained by full geometry optimization at the higher level of electronic structure theory.[31]

3. Results and Discussion

3.1. Overview of the Six H-Abstraction Reactions. Reactions 1−6 represent the H-abstraction reaction of chlorine with methane and a series of five monosubstituted methanes. We can see from Figure 1 and Table 1 that monosubstitution of methane strongly affects both the barriers and the reaction energies. It is important to emphasize that the present calculations apply to isolated gas-phase molecules and that solvation is expected to

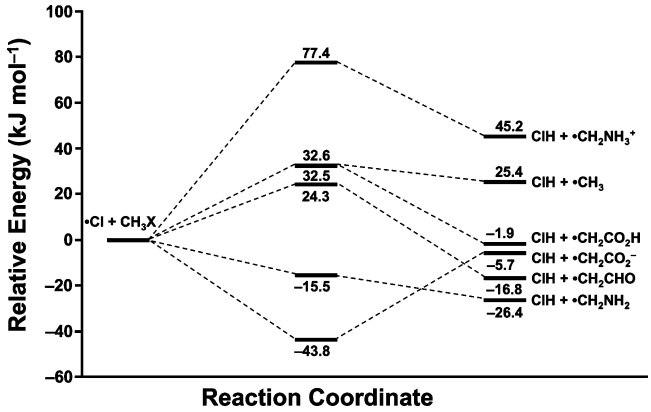

Figure 1. Schematic potential energy profiles for the six H-abstraction reactions. W1′//UQCISD/6-31+G(d,p) energies (kJ mol^{-1}) exclude vibrational contributions. Reactant and product complexes are omitted for simplicity.

modify the reaction energetics, especially for the two reactions involving ionic species. It should also be noted that, while the acetate anion is expected to transfer an electron to the chlorine atom because of the higher EA of $^{\bullet}$Cl,[32,33] we nevertheless restrict our attention to the $^{\bullet}Cl + CH_3CO_2^-$ electronic surface, since this is the reaction relevant to abstraction by $^{\bullet}$Cl from amino acids. Finally, we note that four of the six reactants offer two distinct H-abstraction channels to $^{\bullet}$Cl. For example, $^{\bullet}$Cl can abstract an H-atom from either the methyl group or the amino group of methylamine. Again, as the main goal of the present study is to provide a foundation for future computational studies of $^{\bullet}$Cl reacting with various alkyl-substituted amino acids and peptides, we restrict our calculations to H-abstraction from the methyl carbon of each molecule.

Considering first the reaction energies, we can see from Figure 1 and Table 1 that the parent $^{\bullet}Cl + CH_4 \rightarrow ClH + {}^{\bullet}CH_3$ reaction is predicted to be endothermic by 25.4 kJ mol^{-1}. Substitution with NH_3^+ results in an increased reaction endothermicity, while substitution with each of CO_2H, CO_2^-, CHO, and NH_2 leads to progressively increasing reaction exothermicities. As each of the six H-abstraction reactions shares a common $^{\bullet}$Cl reactant and HCl product, the ordering of reaction energies reflects the stability of the product radicals relative to the corresponding closed-shell reactant molecules. The relative radical stabilities may in turn be rationalized in terms of electronic interactions between the formally singly occupied orbital at the radical center and the various α-substituents. Radical stability is usually measured by the radical stabilization energy (RSE),[34−37] which, for substituted methyl radicals, is generally defined as the enthalpy change for the reaction

$$CH_4 + {}^{\bullet}CH_2X \rightarrow {}^{\bullet}CH_3 + CH_3X \qquad (7)$$

A positive RSE indicates that the substituent stabilizes the radical with respect to the closed-shell parent, while a negative RSE indicates that the substituent destabilizes the radical with respect to the closed-shell parent. At the W1′ level of theory, $^{\bullet}CH_2NH_3^+$ has an RSE of −19.8 kJ mol^{-1}, while $^{\bullet}CH_2CO_2H$, $^{\bullet}CH_2CO_2^-$, $^{\bullet}CH_2CHO$, and $^{\bullet}CH_2NH_2$ have RSEs of +27.3, +31.1, +42.2, and +51.8 kJ mol^{-1}, respectively. These findings are consistent with those from previous studies of α-substituted methyl radicals.[34−37] For example, four patterns of interaction in an α-substituted methyl radical have previously been described.[34] In brief, π-acceptor groups such as CHO and CO_2H stabilize the radical by delocalizing the unpaired electron into the π-system of the substituent; lone-pair donors such as NH_2 stabilize the radical through interaction with the lone pair; groups such as CH_3 stabilize the radical via hyperconjugation; finally electrophilic groups such as NH_3^+ destabilize the radical by inductive electron withdrawal.

α-Substitution confers even greater variation to the H-abstraction barrier heights than to the reaction energies. For example, the barrier for H-abstraction from $CH_3NH_3^+$ is 77.4 kJ mol^{-1}, as compared with 32.6 kJ mol^{-1} for CH_4 and −43.8 kJ mol^{-1} for $CH_3CO_2^-$. Clearly, there is a correlation between the barrier heights and the reaction energies: Substituents that (de)stabilize the product methyl radical in most cases (de)stabilize the incipient methyl radical that is developing in the TS. This correlation is not absolute, however, for the individual systems. For example, while H-abstraction from CH_3CHO is more exothermic than H-abstraction from $CH_3CO_2^-$, −16.8 vs −5.7 kJ mol^{-1}, the former reaction has a barrier of 32.5 kJ mol^{-1}, while the latter possesses no barrier to H-abstraction, relative to separated reactants. We note that negative values for barriers can arise through the presence of reactant and product complexes, which have been omitted from Figure 1 for simplicity but are discussed further in later sections of the paper.

To help understand the patterns of reactivity, we make use of the Pross−Shaik valence-bond (VB) state-correlation or curve-crossing models of radical H-abstraction reactions, which have been utilized previously by several groups to rationalize the properties of the H-abstraction PES in terms of measurable properties of the reactants and products.[27,38,39] In such a treatment, the ground-state H-abstraction potential surface for the reaction of $^{\bullet}$Cl with HR is considered to result from the interaction of the reactant configuration (Cl↑ H↑ ↓R) and product configuration (Cl↑ ↓H ↓R), along with an admixture of charge-transfer configurations (Cl^- HR^+ and Cl^+ HR^-) (Figure 2). The radical H-abstraction barriers can be seen to be influenced by three key factors:

(1) the electronic energies required to uncouple the spins of the two electrons comprising the reactant H−R and product Cl−H bonds. These energies are equivalent to the energy gaps between the singlet ground states and the triplet excited states, ΔE_{ST}, in the reactant and product molecules, respectively, which are in turn related to their respective bond strengths;
(2) the reaction enthalpy, ΔH_0; and
(3) the development of charge-transfer or polar character in the TS, resulting from interaction of the ground-state wave function with low-lying charge-transfer configurations, that in turn depends on the energy gap, $\Delta E_{\text{covalent-ionic}}^{\ddagger}$.

Although the importance of each of these factors varies for differing reactions, previous studies have generally agreed that H-abstraction barriers are lowered for reactions with smaller reactant and product singlet−triplet splittings (ΔE_{ST}), for increasingly exothermic reactions, and for reactions with increasingly low-lying charge-transfer configurations. Several studies have suggested that for electrophilic radicals such as $^{\bullet}$Cl, the TS stabilization afforded by interaction with low-lying charge-transfer configurations is the dominant influence on the H-abstraction barrier height.[27,38] In the lexicon of VB theory, the covalent electronic configuration at the TS is stabilized by interaction with the charge-transfer configuration, that is, $^{\bullet}Cl$ $^{\bullet}H$ $^{\bullet}R \leftrightarrow Cl^-$ $^{\bullet}H$ R^+, and this stabilizing interaction increases as the relative energy of the charge-transfer configuration decreases. We may thus expect for the present reactions that increasingly electron-donating substituents within R will give rise to low-

TABLE 1: Calculated TS Geometries (Å, Degrees)[a] and NBO Charges (Q, e),[b] Energy Differences Between Covalent and Charge-Transfer Configurations (eV),[c] Barriers ($\Delta E^{\ddagger}$, $\Delta H_0^{\ddagger}$, kJ mol^{-1}),[d] and Reaction Energies (ΔE, ΔH_0, kJ mol^{-1})[d] for the Six H-Abstraction Reactions

	r_{Cl-H}	r_{H-C}	r_{Cl-C}	∠Cl−H−C	Q(Cl)[b]	Q(H)[b]	Q(R)[b,e]	IE(•R) − EA(•Cl)[e]	$\Delta E^{\ddagger}$ ($\Delta H_0^{\ddagger}$)[d,f]	ΔE (ΔH_0)[d,f]
•Cl + CH_4	1.435	1.415	2.850	180.0	−0.25	+0.19	+0.07	6.15	32.6 (15.2)	25.4 (3.8)
•Cl + $CH_3NH_3^+$	1.402	1.463	2.814	158.4	−0.14	+0.17	+0.97	12.74	77.4 (56.7)	45.2 (21.9)
•Cl + CH_3CHO	1.480	1.346	2.826	177.2	−0.21	+0.19	+0.03	6.69	24.3 (7.4)	−16.8 (−33.6)
•Cl + CH_3CO_2H	1.461	1.367	2.828	178.5	−0.20	+0.18	+0.02	6.66	32.5 (14.6)	−1.9 (−20.2)
•Cl + $CH_3CO_2^-$	1.415	1.543	2.945	169.2	−0.39	+0.25	−0.87	0.10	−43.8 (−61.4)	−5.7 (−24.8)
•Cl + CH_3NH_2	1.897	1.140	3.036	176.1	−0.17	+0.15	+0.02	3.41	−15.5 (−19.4)[g]	−26.4 (−44.7)

[a] Geometries optimized at the UQCISD/6-31+G(d,p) level of theory. [b] NBO charge analysis in the TSs is based on CCSD/6-311+G(2df,p) electron densities, calculated at UQCISD/6-31+G(d,p) geometries. [c] The difference in vertical IE of isolated, optimized •R and the EA of •Cl, IE(•R) − EA(•Cl), is calculated using the G3X(MP2)-RAD method, at UQCISD/6-31+G(d,p) optimized geometries. [d] Energies calculated at the W1′ level of theory. [e] R denotes the CH_2X component of the various substituted methanes. [f] Values in parentheses include ZPVE corrections calculated at the UQCISD/6-31+G(d,p) level and scaled by 0.9703, which results in barriers ($\Delta H_0^{\ddagger}$) and reaction enthalpies (ΔH_0) at 0 K. [g] UCCSD(T)/6-311+G(3df,2p) IRCMax calculations on a UQCISD/6-31+G(d,p) IRC suggest that there is no first-order saddle point corresponding to a TS for the H-abstraction reaction in this case. The barriers in this table correspond to values obtained from W1′ single-point energies calculated at the UQCISD/6-31+G(d,p) optimized geometries for the reactants and TS.

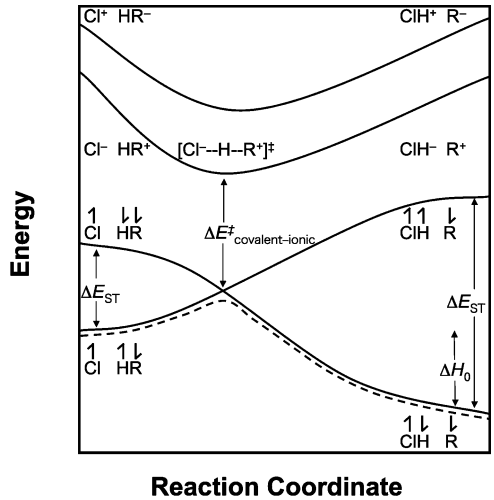

Figure 2. Curve-crossing diagram for the abstraction of hydrogen from RH by chlorine atom. Solid potential energy curves represent the diabatic configurations discussed in the text, while the dashed line represents the ground-state adiabatic potential curve for H-abstraction.

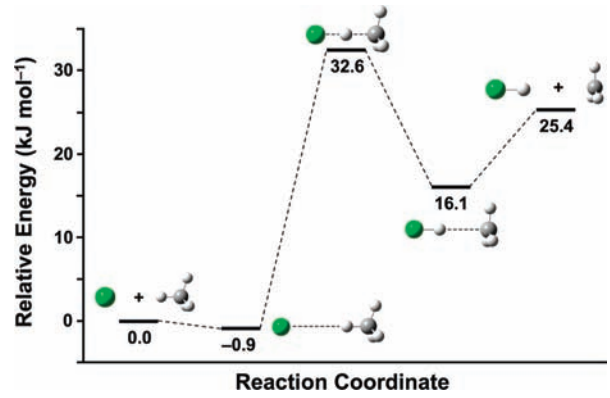

Figure 3. Schematic potential energy profile describing the H-abstraction by chlorine atom from methane. Relative energies (kJ mol^{-1}) are calculated at the W1′//UQCISD/6-31+G(d,p) level and exclude vibrational contributions.

lying charge-transfer states along the H-transfer coordinate, which will result in increasingly stable H-abstraction TSs.

To examine the importance of charge-transfer states, or polarization effects, in determining the H-transfer barriers, we approximate the energy difference between the charge-transfer and covalent configurations of the six TSs as the difference in the vertical IE of optimized, isolated •R and the EA of •Cl, that is, IE(•R) − EA(•Cl) (Table 1).[27] In addition, we also calculate the charge distribution of each TS using the NBO method[26] (Table 1). Considering first the •Cl + CH_4 reaction, we can see that the TS lies 32.6 kJ mol^{-1} above the reactants, has a covalent-ionic state separation of 6.15 eV, and is moderately polarized, with Q(Cl) = −0.25 e, Q(H) = +0.19 e, and Q(CH_3) = +0.06 e. The •Cl + $CH_3NH_3^+$ reaction has a significantly higher barrier of +77.4 kJ mol^{-1}, which most likely arises from destabilization of the TS by inductive withdrawal by the NH_3^+ group. When the •Cl + CH_4, •Cl + CH_3CO_2H, and •Cl + CH_3CHO reactions are compared, we can see the dual influence of charge-transfer stabilization and reaction exothermicity in determining the barrier heights. While the •Cl + CH_3CO_2H and •Cl + CH_3CHO TSs have similar charge-transfer energies (6.66 and 6.69 eV, respectively), the lower barrier for the •Cl + CH_3CHO reaction may be explained by the enhanced •CH_2CHO radical stability and hence increased reaction exothermicity. Despite its endothermicity, the •Cl + CH_4 reaction has a barrier similar to those for the exothermic •Cl + CH_3CO_2H and •Cl + CH_3CHO reactions, which may be explained by the enhanced stabilization afforded to the •Cl + CH_4 TS by its lower-lying charge-transfer configuration (6.15 vs 6.69 and 6.66 eV, respectively). The amino and carboxylate groups of CH_3NH_2 and $CH_3CO_2^-$ are highly electron donating. As a consequence, the •Cl + CH_3NH_2 and •Cl + $CH_3CO_2^-$ TSs have low-lying charge-transfer configurations, of +3.41 and +0.10 eV, respectively. The TS charge-transfer stabilization and reaction exothermicity result in no overall barriers for both of these H-abstraction reactions, which is to say that the [Cl−H−CH_2NH_2]• and [Cl−H−CH_2CO_2]•− TSs lie 15.5 and 43.8 kJ mol^{-1}, respectively, *lower* in energy than the separated reactants.

3.2. Discussion of Individual Reactions and Assessment of Theoretical Methods. ***3.2.1. •Cl + CH_4 → ClH + •CH_3.*** The •Cl + CH_4 → ClH + •CH_3 reaction was studied using the widest set of theoretical methods, as it is the simplest of the six reactions and as both the forward and the reverse reactions have previously been the subject of detailed experimental[4,40] and computational[41,42] investigation. Figure 3 displays the reaction profile at the W1′//UQCISD/6-31+G(d,p) level of theory, including the C_{3v} van der Waals complexes of the reactants and products.

We followed the standard procedure of optimizing molecular geometries with a less expensive level of theory, subsequently using these geometries to calculate final energies with a more

TABLE 2: Effect of Geometry on Forward ($\Delta E_{fwd}^{\ddagger}$) and Reverse ($\Delta E_{rev}^{\ddagger}$) Barriers and Reaction Energies (ΔE) (kJ mol^{-1}) for $^{\bullet}Cl + CH_4 \rightarrow ClH + {}^{\bullet}CH_3$[a,b]

geometry	r_{Cl-H}[c]	r_{H-C}[c]	r_{Cl-C}[c]	$\Delta E_{fwd}^{\ddagger}$	ΔE	$\Delta E_{rev}^{\ddagger}$
UHF/6-31G(d,p)	1.490 (1.435)	1.361 (1.421)	2.851 (2.855)	39.7 (40.5)	32.7	7.0 (7.8)
UHF/6-31+G(d,p)	1.494 (1.439)	1.358 (1.417)	2.852 (2.856)	39.5 (40.4)	32.7	6.9 (7.8)
UHF/6-311+G(d,p)	1.504 (1.438)	1.350 (1.420)	2.853 (2.858)	39.3 (40.4)	32.6	6.7 (7.9)
UHF/6-311+G(3df,2p)	1.505 (1.428)	1.341 (1.424)	2.846 (2.851)	38.9 (40.5)	32.7	6.2 (7.8)
RHF/6-311+G(d,p)	1.516	1.307	2.823	37.5	32.7	4.8
RHF/6-311+G(3df,2p)	1.519	1.297	2.816	37.1	32.8	4.3
UB3-LYP/6-31G(d)	1.374 (1.533)	1.665 (1.428)	3.040 (2.961)	34.4 (45.2)	32.7	1.7 (12.5)
UB3-LYP/6-31+G(d,p)	1.391 (1.514)	1.587 (1.417)	2.977 (2.930)	36.9 (43.0)	32.6	4.3 (10.4)
UB3-LYP/6-311+G(d,p)	1.396 (1.514)	1.568 (1.408)	2.965 (2.922)	37.5 (42.5)	32.6	4.9 (9.9)
UB3-LYP/6-311+G(3df,2p)	1.405 (1.491)	1.524 (1.411)	2.929 (2.902)	38.6 (41.4)	32.4	6.1 (9.0)
UBMK/6-31+G(d,p)	1.394 (1.499)	1.591 (1.425)	2.985 (2.924)	37.0 (42.4)	33.3	3.7 (9.1)
UBMK/6-311+G(3df,2p)	1.411 (1.488)	1.508 (1.404)	2.919 (2.892)	39.0 (41.0)	32.8	6.2 (8.2)
UMP2/6-31G(d)	1.431 (1.456)	1.437 (1.409)	2.869 (2.865)	40.1 (40.3)	32.5	7.7 (7.8)
UMP2/6-31+G(d,p)	1.434 (1.410)	1.393 (1.420)	2.827 (2.830)	40.3 (40.5)	32.5	7.8 (8.0)
UMP2/6-311+G(3df,2p)	1.452 (1.387)	1.358 (1.437)	2.810 (2.824)	40.0 (40.8)	32.5	7.5 (8.4)
UQCISD/6-31G(d)	1.437 (1.487)	1.460 (1.404)	2.897 (2.891)	40.2 (40.9)	32.5	7.7 (8.4)
UQCISD/6-31G(d,p)	1.430 (1.430)	1.421 (1.421)	2.851 (2.851)	40.2 (40.2)	32.5	7.8 (7.8)
UQCISD/6-31+G(d)	1.442 (1.492)	1.457 (1.401)	2.899 (2.893)	40.4 (41.0)	32.5	7.8 (8.5)
UQCISD/6-31+G(d,p)	1.435 (1.435)	1.415 (1.415)	2.850 (2.850)	40.2 (40.2)	32.5	7.7 (7.7)
UQCISD/6-311+G(3df,2p)	1.448 (1.448)	1.396 (1.396)	2.844 (2.844)	40.1 (40.1)	32.4	7.6 (7.6)
UCCSD/6-311+G(3df,2p)	1.449	1.393	2.843	40.1	32.4	7.6
UCCSD(T)/6-311+G(3df,2p)	1.439	1.414	2.854	40.1	32.4	7.7

[a] All relative energies are vibrationless values, calculated at the UCCSD(T)/6-311+G(3df,2p) level, and each forward barrier, $\Delta E_{fwd}^{\ddagger}$, and reaction energy, ΔE, is corrected for the -3.52 kJ mol^{-1} $^{\bullet}Cl$ SO stabilization. [b] The values in parentheses were obtained using the IRCMax procedure from single-point energy calculations at the UCCSD(T)/6-311+G(3df,2p) level. [c] Optimized geometric parameters in the TS.

accurate level of theory.[13,14] The first goal of the assessment study was to determine reliable theoretical methods for the calculation of molecular geometries. Table 2 presents selected geometrical parameters of the H-abstraction TS calculated using a range of methods: the forming Cl−H bond, r_{Cl-H}, the breaking H−C bond, r_{H-C}, and their sum, r_{Cl-C}, which is referred to as the perpendicular looseness.[43] In addition, this table presents reaction energies and forward and reverse barriers, uniformly calculated using UCCSD(T)/6-311+G(3df,2p) single-point energies, with geometries of the reactants, TS, and products optimized at various levels of theory.

First, we examine the variation of the TS geometry that results from varying the one-electron basis set, with a constant level of electron correlation. The same trend is observed across all methods: Increasing the basis set size from 6-31+G(d,p) to 6-311+G(3df,2p) results in a small increase in r_{Cl-H}, a larger decrease in r_{H-C}, and a net decrease in r_{Cl-C}. The opposite behavior is observed when a constant basis set is maintained and the level of electron correlation is increased successively in wave function-based methods from UHF to UCCSD(T): r_{Cl-H} decreases, r_{H-C} increases, and these trends partially cancel for r_{Cl-C}. The opposing changes in TS geometry with increasing basis set and increasing level of correlation also partially cancel. This partial error cancellation leads to reasonable agreement in TS geometry between results from computationally inexpensive wave function-based methods such as UHF/6-31+G(d,p) and UMP2/6-31+G(d,p) and those from computationally demanding methods such as UCCSD(T)/6-311+G(3df,2p). The DFT methods B3-LYP and BMK show the same basis-set dependence as the other methods but tend to underestimate r_{Cl-H} and overestimate r_{H-C}. The TS geometry closest to the UCCSD(T)/6-311+G(3df,2p) benchmark is obtained using the UQCISD/6-31+G(d,p) level of theory, which predicts forming r_{Cl-H} and breaking r_{H-C} bond lengths that differ by just -0.004 and $+0.001$ Å from the benchmark values. We note that inclusion of a set of p-polarization functions on H-atoms is important to attain an accurate TS geometry, that is, the UQCISD/6-31+G(d,p) TS is in better agreement with the benchmark structure than is the UQCISD/6-31+G(d) structure.

The IRCMax procedure has been previously developed to provide good approximations for TS geometries at a high level of theory, without the cost of a full optimization at that level.[31] Table 2 includes the three key bond lengths of the TS, reoptimized using the IRCMax procedure, for 16 of the lower-level methods. Each of the IRCMax calculations employed UCCSD(T)/6-311+G(3df,2p) high-level energies, and thus, each of the resulting IRCMax structural parameters should be compared with the parameters obtained by full optimization at the UCCSD(T)/6-311+G(3df,2p) level. Our results show that IRCMax is most effective, that is, provides the greatest improvement to the TS geometry, at the lower levels of theory whose initial predictions of TS geometry deviate most from the benchmark, namely, UHF, UB3-LYP, and UBMK. In the case of the higher level UMP2, UQCISD, and UCCSD methods, the IRCMax improvements to the TS geometries are more modest.

We next consider the barriers and reaction energies obtained by UCCSD(T)/6-311+G(3df,2p) single-point calculations at the appropriate reactant, TS, and product geometries, which were optimized using 22 different methods. Using UCCSD(T)/6-311+G(3df,2p) geometries, the benchmark forward barrier, reaction energy, and reverse barrier are $\Delta E_{fwd}^{\ddagger} = 40.1$, $\Delta E = 32.4$, and $\Delta E_{rev}^{\ddagger} = 7.7$ kJ mol^{-1}, respectively. The salient finding is that 16 of the 21 other methods yield barriers that fall within ± 1.6 kJ mol^{-1} of the benchmark UCCSD(T) value, while all 21 methods yield reaction energies that fall within ± 1.5 kJ mol^{-1} of the benchmark UCCSD(T) reaction energy. It is important to note that geometries optimized using the inexpensive UHF method with modest basis sets such as 6-31+G(d,p) are sufficiently accurate to ensure that the computed barriers and reaction energies agree with the benchmark values to within ± 1.0 kJ mol^{-1}. In contrast, the ROHF calculations, with both 6-311+G(d,p) and 6-311+G(3df,2p) basis sets, underestimate the TS C−H bond length by ~0.1 Å, which consequently results in underestimation of the forward and reverse barriers by

TABLE 3: Forward ($\Delta E_{fwd}^{\ddagger}$) and Reverse ($\Delta E_{rev}^{\ddagger}$) Barriers and Reaction Energies (ΔE) (kJ mol^{-1}) for the $^{\bullet}Cl + CH_4 \rightarrow ClH + {}^{\bullet}CH_3$ Reaction[a,b]

level of theory	$\Delta E_{fwd}^{\ddagger}$	ΔE	$\Delta E_{rev}^{\ddagger}$
RMP2/6-31+G(d,p)	61.2	47.0	14.3
RMP2/6-311+G(d,p)	49.9	37.0	12.9
RMP2/6-311+G(2df,p)	38.8	33.3	5.6
RMP2/6-311+G(3df,2p)	34.9	28.4	6.5
RMP2/G3XLarge	31.8	24.1	7.7
UQCISD/6-31+G(d,p)	67.0	47.4	19.6
UQCISD/6-311+G(d,p)	56.0	38.2	17.7
UQCISD/6-311+G(2df,p)	52.2	38.9	13.3
UQCISD/6-311+G(3df,2p)	48.3	34.4	13.9
UQCISD/G3XLarge	45.6	29.6	16.1
UHF/6-311+G(3df,2p)	87.5	37.0	50.5
UHF/G3XLarge	90.4	38.0	52.3
UB3-LYP/6-311+G(3df,2p)	21.4	27.2	−5.8
UB3-LYP/G3XLarge	23.8	28.3	−4.5
UBMK/6-311+G(3df,2p)	24.8	30.5	−5.7
UBMK/G3XLarge	26.3	29.6	−3.3
UB2-PLYP/6-311+G(3df,2p)	28.4	28.2	0.2
UB2-PLYP/G3XLarge	29.4	27.5	1.9
UMP2/6-311+G(3df,2p)	37.5	26.9	10.6
UMP2/G3XLarge	34.5	22.3	12.2
UCCSD(T)/6-311+G(3df,2p)	40.2	32.5	7.7
UCCSD(T)/G3XLarge	37.0	27.3	9.7
G3X(MP2)-RAD	34.2	23.3	10.9
W1′	32.6	25.4	7.2
experimental[c]		25.6 ± 0.6	

[a] All relative energies are vibrationless values, and each forward barrier, $\Delta E_{fwd}^{\ddagger}$, and reaction energy, ΔE, is corrected for the −3.52 kJ mol^{-1} $^{\bullet}$Cl SO stabilization. [b] All geometries are optimized at the UQCISD/6-31+G(d,p) level of theory. [c] Vibrationless value; see ref 44.

2.5−3.5 kJ mol^{-1}. The forward and reverse barriers are also underestimated, by up to 7.1 kJ mol^{-1}, when the geometries are optimized using the UB3-LYP and UBMK methods with small basis sets such as 6-31G(d), but agreement is restored to within ±1.6 kJ mol^{-1} of the benchmarks when the optimizations employ the larger 6-311+G(3df,2p) basis set. Finally, agreement with the benchmark barriers and reaction energies to within ±0.2 kJ mol^{-1} is achieved at geometries optimized using the UMP2 and UQCISD methods with modest basis sets such as 6-31G(d) and 6-31+G(d,p). This observation suggests that accurate reaction barriers and energies can be obtained using high-level single-point calculations such as UCCSD(T)/6-311+G(3df,2p) at geometries optimized at modest levels of theory, such as UMP2/6-31+G(d,p), at least for situations where spin contamination is small. The IRCMax procedure was used to calculate the forward and reverse barriers for 15 of the 22 optimization methods, and the results are presented in parentheses in Table 2. For the UMP2 and UQCISD methods, the IRCMax optimizations slightly worsen the agreement with the benchmark barriers, whereas for the DFT methods, the IRCMax procedure leads to geometries and relative energies that are in better agreement with the benchmark.

Having established that UHF, UMP2, and UQCISD methods with modest basis sets can yield accurate geometries for the H-abstraction TSs for the $^{\bullet}Cl + CH_4 \rightarrow ClH + {}^{\bullet}CH_3$ reaction, the second goal was to examine the performance of various electronic structure methods in calculating the barriers and reaction energies. To eliminate effects arising from variation in geometry, we used UQCISD/6-31+G(d,p) geometries throughout. We tested a range of single-level and composite methods in calculating the barriers and reaction energies (Table 3). First, we note the excellent agreement between the benchmark W1′// UQCISD/6-31+G(d,p) reaction energy (ΔE) and experiment: The W1′//UQCISD/6-31+G(d,p) reaction energy underestimates the vibrationless experimental value[22,44−47] of 25.6 ± 0.6 kJ mol^{-1} by just 0.2 kJ mol^{-1}. It is helpful to examine the effect of varying the basis set separately from the effect of varying the level of electron correlation. We can see from Table 3 that there is a large basis set effect. For example, both RMP2/6-31+G(d,p) and UQCISD/6-31+G(d,p) overestimate the W1′ forward barrier and reaction energy by 20−34 kJ mol^{-1}, while overestimating the reverse barrier by just 7−12 kJ mol^{-1}. This error decreases as larger basis sets are used. Thus, RMP2/6-311+G(3df,2p) and RMP2/G3XLarge forward and reverse barriers and reaction energies agree to within 3 kJ mol^{-1} of the benchmark values, while with UQCISD/6-311+G(3df,2p) the overestimation of the forward barriers and reaction energies is reduced to 9−16 kJ mol^{-1}.

Next, we examine the effect of varying the level of electron correlation on the barriers and reaction energies, using the G3XLarge basis set. When the reaction energies are considered, UB3-LYP, UBMK, UB2-PLYP, UMP2, RMP2, UCCSD(T)/G3XLarge, and G3X(MP2)-RAD each calculate SO-corrected ΔE values to within ∼5 kJ mol^{-1} of the +25.4 kJ mol^{-1} W1′ benchmark. The UHF method overestimates ΔE by 12.6 kJ mol^{-1}, while at the UCCSD(T) level, ΔE is overestimated by 1.9 kJ mol^{-1}. UHF overestimates the forward and reverse barriers by 40−60 kJ mol^{-1}, while the UB3-LYP and UBMK methods underestimate these barriers by 6−13 kJ mol^{-1}. This may partly reflect self-interaction error (SIE).[48] Furthermore, both UB3-LYP and UBMK predict that the H-abstraction TS lies between 3 and 6 kJ mol^{-1} *lower* in energy than the ClH + $^{\bullet}CH_3$ products, that is, that there is no overall barrier for the reverse reaction, in contrast to the results of previous experimental and theoretical studies.[42,49] At the B2-PLYP level, the forward barrier is underestimated by just 3.2 kJ mol^{-1}, while the reverse barrier is underestimated by 5.3 kJ mol^{-1}. UMP2, RMP2, UCCSD(T), and G3X(MP2)-RAD each predict forward and reverse barriers that lie within 5 kJ mol^{-1} of the W1′ barriers, while the RMP2/G3XLarge calculations predict forward and reverse barriers within 1 kJ mol^{-1} of the W1′ values. On the other hand, G3X(MP2)-RAD yields forward and reverse barriers that exceed the W1′ values by 1.7 and 3.8 kJ mol^{-1}, respectively. These results suggest that the RMP2/G3XLarge and G3X(MP2)-RAD methods, both of which can be readily applied to our larger systems of interest, perform well when compared with the benchmark W1′ method.

3.2.2. $^{\bullet}Cl + CH_3NH_3^+ \rightarrow ClH + {}^{\bullet}CH_2NH_3^+$. The benchmark method for geometry optimizations for the remaining five reactions was chosen to be UQCISD/6-31+G(d,p), as geometry optimizations at the UCCSD(T)/6-311+G(3df,2p) level of theory are computationally impractical. Figure 4 displays selected stationary points and a schematic energy profile for the $^{\bullet}Cl + CH_3NH_3^+$ reaction, while Table 4 presents selected TS geometrical parameters, barriers, and reaction energies at various levels of theory. Our benchmark calculations predict that the H-abstraction TS lies 77.4 kJ mol^{-1} higher in energy than the separated reactants, has C_s symmetry, and a ∠Cl−H−C of 158.4°. The deviation of ∠Cl−H−C in the TS from 180° may partly reflect electrostatic attraction between the positively charged ammonium group and the polarizable $^{\bullet}$Cl. The W1′ reaction energy of 45.2 kJ mol^{-1} lies within the (quite large) uncertainty limits of the experimental value of 48.1 ± 14.2 kJ mol^{-1}.[46,50−53] Three [$^{\bullet}Cl-CH_3NH_3^+$] reactant complexes and two [$ClH-{}^{\bullet}CH_2NH_3^+$] product complexes were located on the PES. Their full details are presented in the Supporting Information.

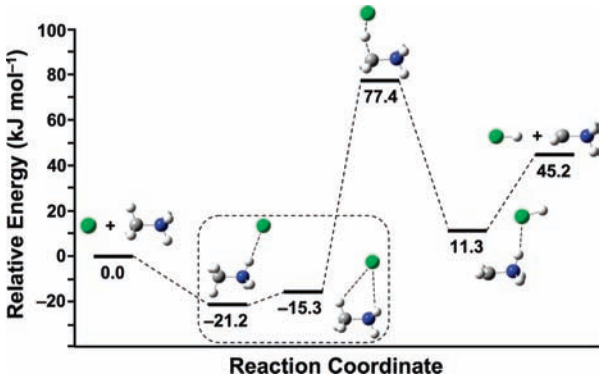

Figure 4. Schematic potential energy profile describing the H-abstraction by chlorine atom from the methylammonium cation. Relative energies (kJ mol^{-1}) are calculated at the W1′//UQCISD/6-31+G(d,p) level and exclude vibrational contributions.[54]

The lowest energy [$^{\bullet}$Cl−$CH_3NH_3^+$] reactant complex lies 21.2 kJ mol^{-1} below the energy of separated reactants, while the representative [ClH−$^{\bullet}CH_2NH_3^+$] product complex lies 33.9 kJ mol^{-1} below the energy of the separated products.[54]

Table 4 includes the three key H-abstraction TS internuclear distances, in addition to the UCCSD(T)/6-311+G(3df,2p) barriers and reaction energies, obtained using geometries optimized at three different levels: UHF/6-31+G(d,p), UB3-LYP/6-31+G(d,p), and UQCISD/6-31+G(d,p). In a similar manner to the findings for $^{\bullet}$Cl + CH_4, UHF/6-31+G(d,p) underestimates the breaking r_{H-C} length by 0.05 Å and overestimates the forming r_{Cl-H} length by 0.04 Å, when compared with the benchmark UQCISD/6-31+G(d,p) values. Conversely, UB3-LYP/6-31+G(d,p) overestimates the breaking r_{H-C} length by 0.09 Å and underestimates the forming r_{Cl-H} length by 0.01 Å. Our UCCSD(T)/6-311+G(3df,2p) single-point calculations at reactant, TS, and product geometries [optimized at the UHF/6-31+G(d,p), UB3-LYP/6-31+G(d,p), and UQCISD/6-31+G(d,p) levels, respectively] show that $\Delta E_{fwd}^{\ddagger}$, $\Delta E_{rev}^{\ddagger}$, and ΔE values calculated at the UHF/6-31+G(d,p) geometries agree with the benchmark to within 0.5 kJ mol^{-1}. UB3-LYP/6-31+G(d,p) geometries perform only slightly less well, with $\Delta E_{fwd}^{\ddagger}$ and $\Delta E_{rev}^{\ddagger}$ values that are 1.3 and 1.5 kJ mol^{-1} lower than the benchmark.

The barriers and reaction energies presented in Table 4 were calculated using UQCISD/6-31+G(d,p) geometries across a range of theoretical levels. In a similar manner to the $^{\bullet}$Cl + CH_4 results, we observe that RMP2/6-31+G(d,p) and UQCISD/6-31+G(d,p) both overestimate the benchmark forward barrier and reaction energy by 20−40 kJ mol^{-1} and that this error is ameliorated by using the larger 6-311+G(3df,2p) and G3XLarge basis sets. We thus examine barriers and reaction energies with a range of methods for treating electron correlation, in conjunction with the G3XLarge basis set. As for $^{\bullet}$Cl + CH_4, UHF/G3XLarge overestimates the $\Delta E_{fwd}^{\ddagger}$ and $\Delta E_{rev}^{\ddagger}$ values by 50−70 kJ mol^{-1}, with respect to the W1′ benchmark. UB3-LYP and UBMK calculate ΔE values that lie within 2.5 kJ mol^{-1} of the benchmark, and $\Delta E_{fwd}^{\ddagger}$ and $\Delta E_{rev}^{\ddagger}$ values that underestimate the benchmark barriers by 4−7 kJ mol^{-1}. The UB2-PLYP reaction energy overestimates the benchmark by just 0.5 kJ mol^{-1}, and the UB2-PLYP forward and reverse barriers underestimate the benchmark barriers by just 1.9 and 2.4 kJ mol^{-1}, respectively. The UMP2, RMP2, and UCCSD(T) methods, along with G3X(MP2)-RAD, tend to overestimate the benchmark $\Delta E_{fwd}^{\ddagger}$ and $\Delta E_{rev}^{\ddagger}$ values by up to 5.8 kJ mol^{-1}, while the reaction energies at these levels agree with the benchmark ΔE to within 2.9 kJ mol^{-1}. As in the case of $^{\bullet}$Cl + CH_4, we note that RMP2/G3XLarge yields reliable $\Delta E_{fwd}^{\ddagger}$, $\Delta E_{rev}^{\ddagger}$, and ΔE values, agreeing to within 1 kJ mol^{-1} of the benchmark values.

3.2.3. $^{\bullet}$Cl + CH_3CHO → ClH + $^{\bullet}CH_2CHO$. The $^{\bullet}$Cl + CH_3CHO encounter presents two channels for H-abstraction, namely, abstraction of the aldehyde H to yield ClH + $CH_3C(^{\bullet})O$, and abstraction of a methyl H to yield ClH + $^{\bullet}CH_2CHO$. Experimental kinetic studies concur that the aldehyde H-abstraction channel dominates (>95%) the reactivity.[55,56] The only study to present electronic structure calculations for these reactions reported a barrier of 3.6 kJ mol^{-1} for the $^{\bullet}$Cl + CH_3CHO → ClH + $CH_3C(^{\bullet})O$ channel, using MP2/aug-cc-pVDZ; results for the methyl H-abstraction channel were not presented.[56] Our study focuses exclusively on the $^{\bullet}$Cl + CH_3CHO → ClH + $^{\bullet}CH_2CHO$ channel, because it is relevant to our ultimate aim of examining hydrogen abstraction from the side chains of amino acids and peptides. Figure 5 displays a schematic W1′//UQCISD/6-31+G(d,p) reaction profile, and Table 5 presents TS geometrical parameters and barriers and reaction energies across a range of levels of theory. As for the previous reactions, the W1′ reaction energy (−16.8 kJ mol^{-1}) is in close agreement with the experimental value[46,53,57,58] of −18.3 ± 10.2 kJ mol^{-1}.

Our results in Table 5 demonstrate that, in comparison with the UQCISD/6-31+G(d,p) benchmark values, UHF/6-31+G(d,p) underestimates the TS r_{H-C} length and overestimates the r_{Cl-H} length, while UB3-LYP/6-31+G(d,p) overestimates the breaking bond length, r_{H-C}, but agrees with UQCISD/6-31+G(d,p) for the length of the forming r_{Cl-H} bond. The results in Table 5 also indicate that barriers and energies calculated using UB3-LYP/6-31+G(d,p) geometries agree to within 0.5 kJ mol^{-1} of the benchmark values, while those calculated using UHF/6-31+G(d,p) geometries agree to within 1.0 kJ mol^{-1} of the benchmark.

When barriers and reaction energies are examined across a range of computational levels, obtained at identical UQCISD/6-31+G(d,p) geometries, some similarities and some differences from the trends observed for $^{\bullet}$Cl + CH_4 and $^{\bullet}$Cl + $CH_3NH_3^+$ are apparent. The basis set effect recurs. Thus, the forward barriers and reaction energies calculated at RMP2/6-31+G(d,p) and UQCISD/6-31+G(d,p) both overestimate the benchmarks by 23−35 kJ mol^{-1}, while RMP2/G3XLarge barriers and energies agree with the benchmark values to within 10 kJ mol^{-1}. Restricting our discussion to results obtained with the G3XLarge basis set, we note that UHF overestimates the benchmark forward and reverse barriers by 62−65 kJ mol^{-1}, while UB3-LYP and UBMK underestimate the benchmark values by 7−14 kJ mol^{-1}. Again, UB2-PLYP outperforms UB3-LYP and UBMK, providing values for $\Delta E_{fwd}^{\ddagger}$ and $\Delta E_{rev}^{\ddagger}$ that underestimate the benchmark by just 4−6 kJ mol^{-1}. Most strikingly, UMP2/G3XLarge overestimates $\Delta E_{fwd}^{\ddagger}$ and ΔE by 32−39 kJ mol^{-1}, due to significant spin contamination in the wave function for the TS and the $^{\bullet}CH_2CHO$ radical product. For example, the UMP2/G3XLarge TS and $^{\bullet}CH_2CHO$ wave functions yield $\langle S^2 \rangle$ values of 0.93 and 0.94, respectively, significantly larger than the ideal value of 0.75. Previous work has demonstrated that the UMP2 method leads to severely spin-contaminated $^{\bullet}CH_2CHO$ electronic wave functions and should thus be avoided for this radical.[34] In contrast, wave functions obtained using spin-restricted methods, such as RMP2, being pure eigenfunctions of the S^2 operator, do not suffer from spin contamination,[13,14] and thus, RMP2 methods are generally superior to UMP2 in calculating reaction energetics involving

TABLE 4: Optimized Geometrical Parameters (Å) for the TS for the Reaction $^{\bullet}Cl + CH_3NH_3^+ \rightarrow ClH + {}^{\bullet}CH_2NH_3^+$, Together with Reaction Energies (ΔE) and Forward ($\Delta E_{fwd}^{\ddagger}$) and Reverse ($\Delta E_{rev}^{\ddagger}$) Barriers (kJ mol^{-1})[a,b]

level of theory	geometry	r_{Cl-H}	r_{H-C}	r_{Cl-C}	$\Delta E_{fwd}^{\ddagger}$	ΔE	$\Delta E_{rev}^{\ddagger}$
UCCSD(T)/6-311+G(3df,2p)	UHF	1.441	1.416	2.831	84.8	52.8	32.0
UCCSD(T)/6-311+G(3df,2p)	UB3-LYP	1.391	1.549	2.867	83.0	52.7	30.3
UCCSD(T)/6-311+G(3df,2p)	UQCISD	1.402	1.463	2.814	84.3	52.5	31.8
UHF/6-311+G(3df,2p)	UQCISD				141.5	58.7	82.8
UHF/G3XLarge	UQCISD				143.9	59.7	84.2
UB3-LYP/6-311+G(3df,2p)	UQCISD				68.1	43.8	24.3
UB3-LYP/G3XLarge	UQCISD				70.1	45.1	25.0
UBMK/6-311+G(3df,2p)	UQCISD				72.3	48.6	23.8
UBMK/G3XLarge	UQCISD				73.0	47.7	25.3
UB2-PLYP/6-311+G(3df,2p)	UQCISD				74.7	46.3	28.5
UB2-PLYP/G3XLarge	UQCISD				75.5	45.7	29.8
UMP2/6-311+G(3df,2p)	UQCISD				83.6	47.2	36.4
UMP2/G3XLarge	UQCISD				80.9	42.8	38.0
RMP2/6-31+G(d,p)	UQCISD				112.0	68.8	43.3
RMP2/6-311+G(3df,2p)	UQCISD				80.8	48.7	32.1
RMP2/G3XLarge	UQCISD				77.9	44.6	33.2
UQCISD/6-31+G(d,p)	UQCISD				116.9	69.1	47.8
UCCSD(T) /6-311+G(3df,2p)	UQCISD				84.3	52.5	31.8
UCCSD(T)/G3XLarge	UQCISD				81.8	47.7	34.1
G3X(MP2)-RAD	UQCISD				80.0	44.7	35.3
W1′	UQCISD				77.4	45.2	32.2
experimental[c]						48.1 ± 14.2	

[a] All relative energies are vibrationless values, and each forward barrier, $\Delta E_{fwd}^{\ddagger}$, and reaction energy, ΔE, is corrected for the −3.52 kJ mol^{-1} $^{\bullet}$Cl SO stabilization. [b] All geometry optimizations employed the 6-31+G(d,p) basis set. [c] Vibrationless value; see ref 50.

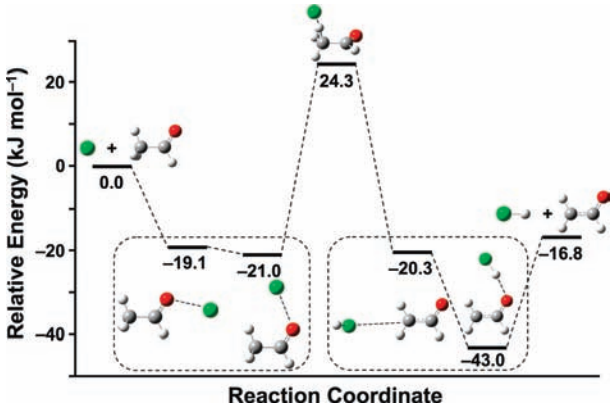

Figure 5. Schematic potential energy profile describing the H-abstraction by chlorine atom from acetaldehyde. Relative energies (kJ mol^{-1}) are calculated at the W1′//UQCISD/6-31+G(d,p) level and exclude vibrational contributions.[54]

open-shell systems. The RMP2/G3XLarge $\Delta E_{fwd}^{\ddagger}$ and $\Delta E_{rev}^{\ddagger}$ values underestimate the benchmark barriers by 5.1 and 8.2 kJ mol^{-1}, respectively, while RMP2/G3XLarge overestimates the benchmark reaction exothermicity by 3.0 kJ mol^{-1}. By contrast, the G3X(MP2)-RAD procedure yields $\Delta E_{fwd}^{\ddagger}$, $\Delta E_{rev}^{\ddagger}$, and ΔE values that agree with the benchmark to within 3 kJ mol^{-1}.

3.2.4. $^{\bullet}Cl + CH_3CO_2H \rightarrow ClH + {}^{\bullet}CH_2CO_2H$. Selected stationary points on the $^{\bullet}Cl + CH_3CO_2H$ PES are displayed in Figure 6, while TS geometrical parameters, barriers, and reaction energies are presented in Table 6. Although $^{\bullet}$Cl may abstract either a methyl H or the carboxylic H from acetic acid, we have only examined the former channel, again because of its relevance to amino acid chemistry. W1′// UQCISD/6-31+G(d,p) calculations predict that the $^{\bullet}Cl + CH_3CO_2H$ reaction has a forward barrier of 32.5 kJ mol^{-1} and a reaction energy of −1.9 kJ mol^{-1}, which agrees closely with the experimental value[32,46,59,60] of −2.4 ± 3.6 kJ mol^{-1}.

The observed dependence of the optimized geometrical parameters in the TS on the method used is similar to that noted for the other reactions. Despite small variations from the UQCISD/6-31+G(d,p) TS geometry, both UHF and UB3-LYP/6-31+G(d,p) geometries yield $\Delta E_{fwd}^{\ddagger}$, $\Delta E_{rev}^{\ddagger}$, and ΔE values that agree with the benchmark to within 0.7 kJ mol^{-1}.

We again note the ∼20−30 kJ mol^{-1} overestimation of the forward barriers and reaction energies obtained using RMP2 and UQCISD with the 6-31+G(d,p) basis set and the closer agreement obtained using the RMP2/G3XLarge method. The UHF/G3XLarge forward and reverse barriers overestimate the benchmarks by 70.4 and 54.1 kJ mol^{-1}, respectively, while the UHF/G3XLarge reaction energy overestimates the benchmark by 16.8 kJ mol^{-1}. As observed for the previous reactions, depending on the functional, DFT yields significantly more accurate results. Thus, the agreement between the DFT and W1′ barriers and reaction energies improves progressively from UB3-LYP to UBMK to UB2P-LYP, whereby the UB2P-LYP reaction energy underestimates the W1′ value by just 0.4 kJ mol^{-1}, while (relative to W1′) the UB2P-LYP barriers are too low by 4−5 kJ mol^{-1}. Consistent with findings for the previous three reactions, G3X(MP2)-RAD yields $\Delta E_{fwd}^{\ddagger}$ and $\Delta E_{rev}^{\ddagger}$ values that fall within 3 kJ mol^{-1} of the benchmark values and a ΔE value that exceeds the benchmark ΔE by just 1 kJ mol^{-1}.

3.2.5. $^{\bullet}Cl + CH_3CO_2^- \rightarrow ClH + {}^{\bullet}CH_2CO_2^-$. As discussed in section 3.1, the EA of $^{\bullet}$Cl (3.61 eV)[32] exceeds that of $CH_3CO_2^{\bullet}$ (3.25 eV),[33] and thus, a gas-phase encounter between $^{\bullet}$Cl and $CH_3CO_2^-$ is expected to lead to electron transfer to form Cl^- and $CH_3CO_2^{\bullet}$. However, in the present study, we restrict our attention to the $^{\bullet}Cl + CH_3CO_2^-$ reaction, again so as to maintain relevance to amino acid and peptide chemistry. The $^{\bullet}Cl + CH_3CO_2^-$ potential energy profile, displayed in Figure 7, is qualitatively different to those of the four preceding reactions, as the charge-induced dipole interaction between $CH_3CO_2^-$ and $^{\bullet}$Cl is strongly attractive. The striking feature of the PES is that the H-abstraction TS energy lies 43.8 kJ mol^{-1} *below* that of the $^{\bullet}Cl + CH_3CO_2^-$ reactants and 38.1 kJ mol^{-1} *below* that of the $ClH + {}^{\bullet}CH_2CO_2^-$ products. It is important to note that an H-abstraction TS is nevertheless located as a first-order saddle

TABLE 5: Optimized Geometrical Parameters (Å) for the TS for the Reaction $^{\bullet}Cl + CH_3CHO \rightarrow ClH + {}^{\bullet}CH_2CHO$, Together with Reaction Energies (ΔE) and Forward ($\Delta E_{fwd}^{\ddagger}$) and Reverse ($\Delta E_{rev}^{\ddagger}$) Barriers (kJ mol^{-1})[a,b]

level of theory	geometry	r_{Cl-H}	r_{H-C}	r_{Cl-C}	$\Delta E_{fwd}^{\ddagger}$	ΔE	$\Delta E_{rev}^{\ddagger}$
UCCSD(T)/6-311+G(3df,2p)	UHF	1.536	1.320	2.855	30.8	−8.4	39.3
UCCSD(T)/6-311+G(3df,2p)	UB3-LYP	1.480	1.393	2.868	31.4	−7.0	38.4
UCCSD(T)/6-311+G(3df,2p)	UQCISD	1.480	1.346	2.826	31.5	−7.4	38.9
UHF/6-311+G(3df,2p)	UQCISD				86.6	−13.9	100.5
UHF/G3XLarge	UQCISD				89.6	−13.1	102.7
UB3-LYP/6-311+G(3df,2p)	UQCISD				7.7	−24.2	32.0
UB3-LYP/G3XLarge	UQCISD				10.3	−23.1	33.4
UBMK/6-311+G(3df,2p)	UQCISD				16.0	−16.9	32.8
UBMK/G3XLarge	UQCISD				16.8	−17.2	34.1
UB2-PLYP/6-311+G(3df,2p)	UQCISD				18.8	−14.4	33.1
UB2-PLYP/G3Xlarge	UQCISD				20.2	−15.0	35.2
UMP2/6-311+G(3df,2p)	UQCISD				59.1	26.8	32.3
UMP2/G3XLarge	UQCISD				56.7	22.0	34.7
RMP2/6-31+G(d,p)	UQCISD				47.3	9.4	37.9
RMP2/6-311+G(3df,2p)	UQCISD				21.4	−9.6	31.0
RMP2/G3XLarge	UQCISD				19.2	−13.8	33.0
UQCISD/6-31+G(d,p)	UQCISD				58.8	6.8	51.9
UCCSD(T)/6-311+G(3df,2p)	UQCISD				31.5	−7.4	38.9
UCCSD(T)/G3XLarge	UQCISD				29.2	−12.6	41.8
G3X(MP2)-RAD	UQCISD				23.9	−19.6	43.5
W1′	UQCISD				24.3	−16.8	41.2
experimental[c]						−18.3 ± 10.2	

[a] All relative energies are vibrationless values, and each forward barrier, $\Delta E_{fwd}^{\ddagger}$, and reaction energy, ΔE, is corrected for the −3.52 kJ mol^{-1} $^{\bullet}$Cl SO stabilization. [b] All geometry optimizations employed the 6-31+G(d,p) basis set. [c] Vibrationless value; see ref 57.

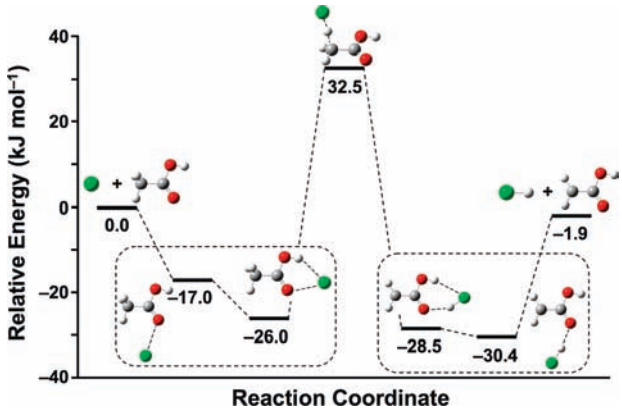

Figure 6. Schematic potential energy profile describing the H-abstraction by chlorine atom from acetic acid. Relative energies (kJ mol^{-1}) are calculated at the W1′//UQCISD/6-31+G(d,p) level and exclude vibrational contributions.[54]

point using each of the UHF, UB3-LYP, and UQCISD/6-31+G(d,p) levels of theory. The W1′ procedure predicts a reaction energy of −5.7 kJ mol^{-1}, which may be compared with an estimate from experimental data[32,46,53,61,62] of −17.2 ± 14.2 kJ mol^{-1}, with quite a large experimental uncertainty. Figure 7 also shows that the PES supports two strongly bound reactant complexes. We note in particular the reactant complex displaying a $^{\bullet}$Cl−carbonyl oxygen interaction that leads to a binding energy of 115.6 kJ mol^{-1}. No stationary point corresponding to a [ClH−$^{\bullet}CH_2CO_2^-$] product complex was located. IRC and gradient-based optimizations showed that, following H-abstraction, HCl migrates toward the carboxylate region of the $^{\bullet}CH_2CO_2^-$ radical and transfers its proton to yield the [$^{\bullet}CH_2CO_2H$−Cl$^-$] complex, which is the global minimum.

Both the shape of the $^{\bullet}Cl + CH_3CO_2^-$ PES and the location of the H-abstraction TS on the PES depend sensitively on the level of theory. We restrict the present discussion to calculations using the G3XLarge basis set. Each of the hybrid DFT methods and the conventional correlated methods agree that the energy of the H-abstraction TS lies 36−62 kJ mol^{-1} below the energy of $^{\bullet}Cl + CH_3CO_2^-$, while UHF/G3XLarge calculations predict a barrier of 32.1 kJ mol^{-1}. Table 7 shows that there is significant variation in the optimized r_{Cl-H}, r_{H-C}, and r_{Cl-C} internuclear distances at the UHF, UB3-LYP, and UQCISD/6-31+G(d,p) levels. The UHF/6-31+G(d,p) geometry underestimates the benchmark UQCISD/6-31+G(d,p) value for r_{H-C} by 0.21 Å and overestimates the benchmark r_{Cl-H} value by 0.14 Å. UB3-LYP/6-31+G(d,p) overestimates the benchmark r_{H-C} value by 0.5 Å and underestimates the benchmark r_{Cl-H} value by 0.08 Å. The large variation in TS geometry is reflected in the barriers, as calculated using UCCSD(T)/6-311+G(3df,2p) at the three different lower-level geometries. While the UHF and UB3-LYP geometries result in excellent (0.5 kJ mol^{-1}) agreement with the benchmark ΔE, the UHF and UB3-LYP geometries furnish barriers that underestimate the benchmark by ∼10 kJ mol^{-1}.

As with the preceding reactions, forward barriers and reaction energies calculated using RMP2/6-31+G(d,p) and UQCISD/6-31+G(d,p) overestimate the benchmarks by 20−40 kJ mol^{-1}, while agreement with the benchmark barriers and reaction energies is restored to 2−7 kJ mol^{-1} using RMP2/G3XLarge. UHF/G3XLarge overestimates the forward and reverse barriers by 75.9 and 56.6 kJ mol^{-1}, respectively, and the reaction energy by 19.3 kJ mol^{-1}. The DFT/G3XLarge levels provide reaction energies that agree with the benchmark value to within 2.7 kJ mol^{-1}, while the conventional correlated methods perform reasonably well, yielding barriers and reaction energies that agree with the benchmark to within 7.1 kJ mol^{-1}. The closest agreement with W1′ is obtained using G3X(MP2)-RAD, which provides both reaction and TS energies (relative to reactants) that agree with the benchmark values to within 2.7 kJ mol^{-1}.

3.2.6. $^{\bullet}Cl + CH_3NH_2 \rightarrow ClH + {}^{\bullet}CH_2NH_2$. The chemical reaction dynamics and PES for the $^{\bullet}Cl + CH_3NH_2$ reactions have been measured and calculated, respectively, by Orr-Ewing and co-workers.[64] Spectroscopic interrogation of the HCl product enabled them to determine that the branching ratio between the two H-abstraction channels

TABLE 6: Optimized Geometrical Parameters (Å) for the TS for the Reaction $^{\bullet}Cl + CH_3CO_2H \rightarrow ClH + {}^{\bullet}CH_2CO_2H$, Together with Reaction Energies (ΔE) and Forward ($\Delta E_{fwd}^{\ddagger}$) and Reverse ($\Delta E_{rev}^{\ddagger}$) Barriers (kJ mol^{-1})[a,b]

level of theory	geometry	r_{Cl-H}	r_{H-C}	r_{Cl-C}	$\Delta E_{fwd}^{\ddagger}$	ΔE	$\Delta E_{rev}^{\ddagger}$
UCCSD(T)/6-311+G(3df,2p)	UHF	1.504	1.347	2.850	38.7	6.4	32.3
UCCSD(T)/6-311+G(3df,2p)	UB3-LYP	1.454	1.429	2.880	37.8	6.7	31.0
UCCSD(T)/6-311+G(3df,2p)	UQCISD	1.461	1.367	2.828	38.2	6.4	31.7
UHF/6-311+G(3df,2p)	UQCISD				100.0	13.5	86.4
UHF/G3XLarge	UQCISD				102.9	14.4	88.5
UB3-LYP/6-311+G(3df,2p)	UQCISD				18.2	−7.4	25.6
UB3-LYP/G3XLarge	UQCISD				20.8	−6.2	27.0
UBMK/6-311+G(3df,2p)	UQCISD				24.9	0.0	24.9
UBMK/G3XLarge	UQCISD				26.7	−0.7	27.3
UB2-PLYP/6-311+G(3df,2p)	UQCISD				26.4	−1.8	28.1
UB2-PLYP/G3Xlarge	UQCISD				27.8	−2.3	30.2
UMP2/6-311+G(3df,2p)	UQCISD				40.6	11.1	29.4
UMP2/G3XLarge	UQCISD				38.4	6.6	31.8
RMP2/6-31+G(d,p)	UQCISD				55.3	24.7	30.6
RMP2/6-311+G(3df,2p)	UQCISD				29.5	4.0	25.5
RMP2/G3XLarge	UQCISD				27.2	−0.1	27.3
UQCISD/6-31+G(d,p)	UQCISD				66.2	23.5	42.8
UCCSD(T)/6-311+G(3df,2p)	UQCISD				38.2	6.4	31.7
UCCSD(T)/G3XLarge	UQCISD				35.9	1.5	34.4
G3X(MP2)-RAD	UQCISD				35.2	−0.9	36.0
W1′	UQCISD				32.5	−1.9	34.4
experimental[c]						−2.4 ± 3.6	

[a] All relative energies are vibrationless values, and each forward barrier, $\Delta E_{fwd}^{\ddagger}$, and reaction energy, ΔE, is corrected for the −3.52 kJ mol^{-1} $^{\bullet}$Cl SO stabilization. [b] All geometry optimizations employed the 6-31+G(d,p) basis set. [c] See ref 59.

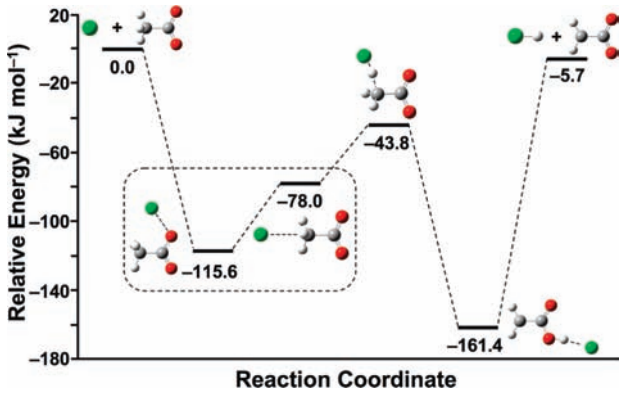

Figure 7. Schematic potential energy profile describing the H-abstraction by chlorine atom from the acetate anion. Relative energies (kJ mol^{-1}) are calculated at the W1′//UQCISD/6-31+G(d,p) level and exclude vibrational contributions.[54]

$$^{\bullet}Cl + CH_3NH_2 \rightarrow ClH + {}^{\bullet}CH_2NH_2 \quad (8)$$

$$^{\bullet}Cl + CH_3NH_2 \rightarrow ClH + CH_3NH^{\bullet} \quad (9)$$

was approximately 1:1 and that HCl produced via the aminomethyl channel (reaction 8) departed with significant rotational excitation, while HCl produced via the methanaminyl channel (reaction 9) did not. They suggested that electrostatic interaction between the nascent HCl and the two product organic radicals gave rise to the two different patterns of HCl rotational excitation.

The present study restricts its focus to H-abstraction from the methyl group (reaction 8). Selected stationary points from the W1′//UQCISD/6-31+G(d,p) PES are displayed in Figure 8, and relevant TS geometrical parameters and barriers and reaction energies are summarized in Table 8. First, we note that the W1′ reaction energy (−26.4 kJ mol^{-1}) agrees well with the experimental value[45,51,53,65] of −23.8 ± 8.5 kJ mol^{-1}. The present W1′//UQCISD/6-31+G(d,p) results also agree broadly with the G2//MP2/6-311G(d,p) results of Orr-Ewing et al.[46,51,60] As in the previous study, the energy of the methyl H-abstraction TS lies below the energy of the reactants, the H-abstraction reaction is exothermic, and the W1′//UQCISD PES supports several reactant and product complexes. The global minimum is a $[CH_3NH_2-{}^{\bullet}Cl]$ complex with a two-center, three-electron N−Cl bond (r_{Cl-N} = 2.414 Å), lying 64.4 kJ mol^{-1} below the energy of the reactants.

In addition to the TS for H-abstraction with C_1 symmetry reported by Orr-Ewing et al.,[64] we located a lower energy C_s H-abstraction TS, in which the incipient HCl is *syn* to the N−H bonds and *antiperiplanar* to the σ-orbital of the nitrogen lone pair. This structure has an energy 15.5 kJ mol^{-1} below that of the reactants. In conjunction with the 6-31+G(d,p) and 6-311+G(d,p) basis sets, each of the UHF, UMP2, RMP2, and UQCISD methods are able to locate a first-order saddle point corresponding to the C_s TS for methyl H-abstraction (Figure 8).

Table 8 shows that as higher orders of electron correlation are included in the calculations, for example, UHF → UMP2 → UCCSD(T), the relative energy of the H-abstraction TS decreases. This prompts the question as to whether a first-order H-abstraction saddle point exists on the UCCSD(T) PES or whether the energy monotonically decreases along the H-transfer reaction path. Geometry optimization at the UCCSD(T)/6-31G(d) level is able to locate a C_s methyl H-abstraction saddle point, but UCCSD(T) optimizations using 6-31+G(d,p) and 6-311+G(2df,p) fail to locate an analogous methyl H-abstraction TS. Unfortunately, UCCSD(T) geometry optimizations using larger basis sets were not feasible. To further investigate the PES in the region of the H-abstraction TS, UCCSD(T)/6-311+G(3df,2p) single-point calculations were carried out along the C_s methyl H-abstraction path, using a UHF/6-31+G(d,p) IRC, and along a C_1 methyl H-abstraction path using a UMP2/6-31+G(d,p) IRC. Both of these UCCSD(T)/6-311+G(3df,2p) PES slices decrease monotonically from the $^{\bullet}Cl + HCH_2NH_2$ reactants to the $[ClH-{}^{\bullet}CH_2NH_2]$ complexes, which suggests that there is no first-order saddle point for H-abstraction from the methyl group of methylamine along either of the two pathways

TABLE 7: Optimized Geometrical Parameters (Å) for the TS for the Reaction $^{\bullet}Cl + CH_3CO_2^- \rightarrow ClH + {}^{\bullet}CH_2CO_2^-$, Together with Reaction Energies (ΔE) and Forward ($\Delta E_{fwd}^{\ddagger}$) and Reverse ($\Delta E_{rev}^{\ddagger}$) Barriers (kJ mol^{-1})[a-c]

level of theory	geometry	r_{Cl-H}	r_{H-C}	r_{Cl-C}	$\Delta E_{fwd}^{\ddagger}$	ΔE	$\Delta E_{rev}^{\ddagger}$
UCCSD(T)/6-311+G(3df,2p)	UHF	1.553	1.332	2.861	−44.7	2.6	−47.3
UCCSD(T)/6-311+G(3df,2p)	UB3-LYP	1.340	2.040	3.308	−45.9	2.1	−48.0
UCCSD(T)/6-311+G(3df,2p)	UQCISD	1.415	1.543	2.945	−36.3	2.1	−38.5
UHF/6-311+G(3df,2p)	UQCISD				28.9	12.5	16.4
UHF/G3XLarge	UQCISD				32.1	13.6	18.5
UB3-LYP/6-311+G(3df,2p)	UQCISD				−64.6	−9.1	−55.5
UB3-LYP/G3XLarge	UQCISD				−62.0	−7.8	−54.2
UBMK/6-311+G(3df,2p)	UQCISD				−51.4	−2.7	−48.7
UBMK/G3XLarge	UQCISD				−49.6	−3.0	−46.6
UB2-PLYP/6-311+G(3df,2p)	UQCISD				−52.7	−5.3	−47.4
UB2-PLYP/G3Xlarge	UQCISD				−52.1	−5.7	−46.4
UMP2/6-311+G(3df,2p)	UQCISD				−32.8	−0.2	−32.6
UMP2/G3XLarge	UQCISD				−36.8	−4.4	−32.5
RMP2/6-31+G(d,p)	UQCISD				−7.4	21.1	−28.5
RMP2/6-311+G(3df,2p)	UQCISD				−32.7	0.5	−33.2
RMP2/G3XLarge	UQCISD				−36.7	−3.4	−33.3
UQCISD/6-31+G(d,p)	UQCISD				−12.5	19.5	−32.0
UCCSD(T)/6-311+G(3df,2p)	UQCISD				−36.3	2.1	−38.5
UCCSD(T)/G3XLarge	UQCISD				−41.6	−2.5	−39.1
G3X(MP2)-RAD	UQCISD				−43.9	−8.4	−35.5
W1′	UQCISD				−43.8	−5.7	−38.1
experimental[d]						−17.2 ± 14.9	

[a] All relative energies are vibrationless values, and each forward barrier, $\Delta E_{fwd}^{\ddagger}$, and reaction energy, ΔE, is corrected for the −3.52 kJ mol^{-1} $^{\bullet}$Cl SO stabilization. [b] All geometry optimizations employed the 6-31+G(d,p) basis set. [c] Present calculations are based on a planar C_{2v} $^{\bullet}CH_2CO_2^-$ radical anion.[63] [d] Vibrationless value; see ref 62.

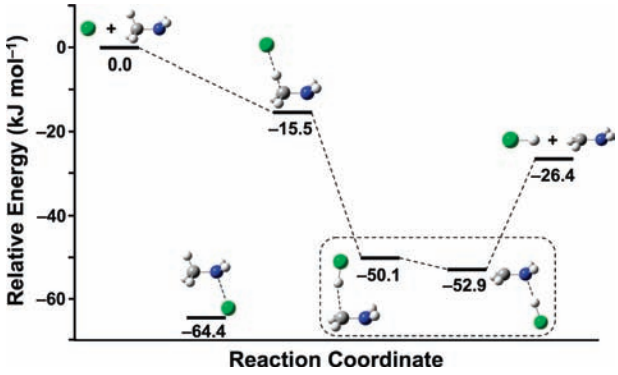

Figure 8. Schematic potential energy profile describing the H-abstraction by chlorine atom from methylamine. Relative energies (kJ mol^{-1}) are calculated at the W1′//UQCISD/6-31+G(d,p) level and exclude vibrational contributions.[54]

examined. It is noteworthy that both UB3-LYP and UBMK, in conjunction with the 6-31+G(d,p) and 6-311+G(d,p) basis sets, calculate barrierless H-abstraction reaction paths and identify the C_s $[Cl-H-CH_2NH_2]^{\bullet}$ configuration as a *local minimum* (a structure having all real vibrational frequencies), with $r_{Cl-H} \sim 1.6$ Å and $r_{H-C} \sim 1.3$ Å.

Two $[ClH-{}^{\bullet}CH_2NH_2]$ product complexes were located at the UQCISD/6-31+G(d,p) level and are included in Figure 8. Following H-abstraction, the minimum energy path leads to a C_s complex, having HCl oriented toward the radical carbon, with an energy 50.1 and 23.7 kJ mol^{-1} below the energies of the reactants and products, respectively. The second product complex also has C_s symmetry but in this case has HCl oriented toward the nitrogen lone pair, with an energy 52.9 and 26.5 kJ mol^{-1} below the energies of the reactants and products, respectively.

It is important to recognize that if indeed the UCCSD(T)/6-311+G(3df,2p) energy monotonically decreases from the $^{\bullet}Cl + CH_3NH_2$ reactants to the $[ClH-{}^{\bullet}CH_2NH_2]$ complexes, the UHF/6-31+G(d,p) and UQCISD/6-31+G(d,p) TSs do not define stationary points on the UCCSD(T) surface but instead define arbitrary points along the C_s H-abstraction reaction path. We nevertheless calculate the potential energy of the UQCISD/6-31+G(d,p) TS using a range of methods, to assess the dependence of the PES topology on level of theory. At the W1′// UQCISD level, the energy of the reference point lies 15.5 kJ mol^{-1} below the energy of the $^{\bullet}Cl + CH_3NH_2$ reactants and 10.9 kJ mol^{-1} above the energy of the $ClH + {}^{\bullet}CH_2NH_2$ products. By contrast, the UHF calculations erroneously predict the H-abstraction pathway to possess both forward and reverse barriers, consistent with their uniform overestimation of barriers, as well as incorrectly predicting the reaction to be endothermic. The UB3-LYP, UBMK, UB2P-LYP, UMP2, and RMP2 methods each predict barrierless forward H-abstraction reactions, as well as reaction energies that agree with the benchmark value to within 6 kJ mol^{-1}. Finally, both UCCSD(T)/G3XLarge and G3X(MP2)-RAD yield barrierless forward H-abstraction reactions, along with reaction energies that agree with the benchmark to within 3.9 kJ mol^{-1}.

3.3. Assessment of Methods across the Six Reactions. Having examined the performance of a range of electronic structure methods across the six reactions independently, it is important to assess their performance on the six reactions collectively. Table 9 collates $\Delta E_{fwd}^{\ddagger}$, $\Delta E_{rev}^{\ddagger}$, and ΔE values, for the six reactions, across the UB3-LYP, UBMK, UB2-PLYP, UMP2, RMP2, UCCSD(T), G3X(MP2)-RAD, and W1′ levels of theory and presents the mean deviations (MD), mean absolute deviations (MAD), and largest deviations (LD) from the benchmark W1′ values. As we find that the use of smaller basis sets such as 6-31+G(d,p) leads to forward barriers and reaction energies that consistently overestimate the benchmarks by 20−40 kJ mol^{-1}, each of the UB3-LYP, UBMK, UB2-PLYP, UMP2, RMP2, and UCCSD(T) values presented in Table 9 refer to results obtained with the large G3XLarge basis set,[30] to limit errors arising from basis set incompleteness. We exclude the "barriers" for the $^{\bullet}Cl + CH_3NH_2$ and $^{\bullet}Cl + CH_3CO_2^-$ reactions from the present analysis, as both of these H-abstraction

TABLE 8: Optimized Geometrical Parameters (Å) for the TS for the Reaction $^{\bullet}Cl + CH_3NH_2 \rightarrow ClH + {}^{\bullet}CH_2NH_2$, Together with Reaction Energies (ΔE) and Forward ($\Delta E_{fwd}^{\ddagger}$ and Reverse ($\Delta E_{rev}^{\ddagger}$) Barriers (kJ mol^{-1})[a,b]

level of theory	geometry	r_{C-H}	r_{H-Cl}	r_{C-Cl}	$\Delta E_{fwd}^{\ddagger}$	ΔE	$\Delta E_{rev}^{\ddagger}$
UCCSD(T)/6-311+G(3df,2p)	UHF	1.248	1.646	2.894	−25.7	−18.2	−7.5
UCCSD(T)/6-311+G(3df,2p)	UQCISD	1.140	1.897	3.036	−13.0	−17.7	4.8
UHF/6-311+G(3df,2p)	UQCISD				32.9	2.0	30.9
UHF/G3XLarge	UQCISD				34.8	2.9	31.9
UB3-LYP/6-311+G(3df,2p)	UQCISD				−53.9	−32.0	−21.9
UB3-LYP/G3XLarge	UQCISD				−52.3	−31.0	−21.2
UBMK/6-311+G(3df,2p)	UQCISD				−39.7	−28.1	−11.6
UBMK/G3XLarge	UQCISD				−38.1	−28.9	−9.2
UB2-PLYP/6-311+G(3df,2p)	UQCISD				−34.6	−27.8	−6.8
UB2-PLYP/G3Xlarge	UQCISD				−33.9	−28.5	−5.4
UMP2/6-311+G(3df,2p)	UQCISD				−5.5	−22.7	17.2
UMP2/G3XLarge	UQCISD				−5.8	−27.0	21.2
RMP2/6-31+G(d,p)	UQCISD				5.5	−0.4	5.8
RMP2/6-311+G(3df,2p)	UQCISD				−5.2	−21.4	16.2
RMP2/G3XLarge	UQCISD				−5.3	−25.5	20.1
UQCISD/6-31+G(d,p)	UQCISD				2.0	1.7	0.3
UCCSD(T)/6-311+G(3df,2p)	UQCISD				−13.0	−17.7	4.8
UCCSD(T)/G3XLarge	UQCISD				−14.8	−22.5	7.8
G3X(MP2)-RAD	UQCISD				−12.2	−24.2	12.0
W1′	UQCISD				−15.5	−26.4	10.9
experimental[c]						−23.8 ± 8.5	

[a] All relative energies are vibrationless values, and each forward barrier, $\Delta E_{fwd}^{\ddagger}$, and reaction energy, ΔE, is corrected for the −3.52 kJ mol^{-1} •Cl SO stabilization. [b] All geometry optimizations employed the 6-31+G(d,p) basis set. [c] Vibrationless value; see ref 65.

reactions have "negative barriers"; that is, the TS energies lie below those of the reactants.

Comparison of the MD, MAD, and LD values in Table 9 shows that the G3X(MP2)-RAD procedure produces the closest agreement with W1′. The MADs for $\Delta E_{fwd}^{\ddagger}$, $\Delta E_{rev}^{\ddagger}$, and ΔE are just 1.8, 2.7, and 1.9 kJ mol^{-1}, respectively, and the LDs for $\Delta E_{fwd}^{\ddagger}$, $\Delta E_{rev}^{\ddagger}$, and ΔE are just 2.7, 3.7, and −2.8 kJ mol^{-1}, respectively. This leads us to recommend G3X(MP2)-RAD as an alternative benchmark method for similar reactions when the W1′ procedure is too expensive.

The UCCSD(T)/G3XLarge and RMP2/G3XLarge methods provide results that rank next in reliability. Both methods yield $\Delta E_{fwd}^{\ddagger}$ and $\Delta E_{rev}^{\ddagger}$ values of comparable accuracy, but RMP2/G3XLarge calculates slightly better reaction energies than UCCSD(T)/G3XLarge. Excluding the two barrierless reactions and considering just the four reactions possessing reaction barriers, it is observed that UCCSD(T)/G3XLarge usually overestimates barriers, by 1−5 kJ mol^{-1}, whereas RMP2/G3XLarge tends to underestimate barriers, by as much as 8 kJ mol^{-1}. Averaging over the four reactions with barriers, the RMP2/G3XLarge method produces MADs for $\Delta E_{fwd}^{\ddagger}$, $\Delta E_{rev}^{\ddagger}$, and ΔE of 3.0, 4.2, and 1.7 kJ mol^{-1}. We thus recommend RMP2/G3XLarge as an economical benchmark procedure for reactions too large to be easily handled by UCCSD(T)/G3XLarge or G3X(MP2)-RAD.

As discussed in section 3.2.3, spin contamination of the TS and product radical wave functions significantly affects UMP2 calculations for the $^{\bullet}Cl + CH_3CHO \rightarrow ClH + {}^{\bullet}CH_2CHO$ reaction and, to a lesser extent, the $^{\bullet}Cl + CH_3CO_2H \rightarrow ClH + {}^{\bullet}CH_2CO_2H$ reaction. As a result, UMP2 calculations overestimate the energy of both the TS and the product radical, inflating the $\Delta E_{fwd}^{\ddagger}$ and ΔE values by up to 39 kJ mol^{-1}. The spin contamination is less marked, however, for the reactions of $^{\bullet}Cl$ with CH_4, $CH_3NH_3^+$, $CH_3CO_2^-$, and CH_3NH_2. Averaged over the relevant reactions, UMP2/G3XLarge produces MADs for $\Delta E_{fwd}^{\ddagger}$, $\Delta E_{rev}^{\ddagger}$, and ΔE of 10.9, 4.9, and 9.1 kJ mol^{-1}, respectively.

Each of the hybrid and double hybrid DFT methods systematically underestimates the barriers, while the performance of these methods improves in the order UB3-LYP, UBMK, and UB2P-LYP. UB3-LYP $\Delta E_{fwd}^{\ddagger}$ and $\Delta E_{rev}^{\ddagger}$ have MADs from the benchmark values of 10.4 and 8.5 kJ mol^{-1}, and the UB3-LYP reaction energies demonstrates a 3.4 kJ mol^{-1} MAD from the benchmarks. UBMK offers more accurate results, with MADs of 6.0 and 7.9 kJ mol^{-1} from the benchmark forward and reverse barriers and a 2.3 kJ mol^{-1} MAD from the benchmark reaction energies. UB2-PLYP provides results that are nearly as accurate as RMP2, producing MADs of just 3.5 and 4.5 kJ mol^{-1} from the benchmark forward and reverse barriers and 1.2 kJ mol^{-1} from the benchmark reaction energies.

4. Conclusions

We have carried out a high-level computational investigation of the abstraction of hydrogen by chlorine atom from methane and five monosubstituted methanes, chosen to reflect the chemical functionalities contained in amino acids and peptides. The first goal of the present study was to calculate benchmark barriers and reaction energies for the six reactions, and as such, our W1′//UQCISD/6-31+G(d,p) calculations reveal a wide variation in the topology of the PESs across the six reactions. The reactions range from being strongly endothermic to exothermic; some possess moderate to high H-abstraction barriers, while others are barrierless to H-abstraction. Charge-polarization and electrostatic interactions shape the PESs to varying degrees, and two of the reactions are prone to significant spin contamination. The trends in the reaction energies reflect the stabilities of the product radicals with respect to their corresponding parent molecules, which are largely determined by electronic interactions between the formally singly occupied orbital at the radical carbon and the various α-substituents. The curve-crossing model for H-abstraction reactions provides an effective rationalization for the widely ranging H-abstraction barrier heights. Within this model, our calculations suggest that two effects appear to control the barrier heights. Barrier heights are progressively lower for reactions that possess low-lying charge-transfer configurations in the vicinity of the TS and

TABLE 9: Comparison of Barriers and Reaction Energies (kJ mol^{-1}) Calculated at Selected Levels of Theory for the Six Hydrogen-Atom Abstraction Reactions[a,b]

	UB3-LYP/ G3XLarge	UBMK/ G3XLarge	UMP2/ G3XLarge	UB2-PLYP/ G3XLarge	RMP2/ G3XLarge	UCCSD(T)/ G3XLarge	G3X(MP2)-RAD	W1′
				$^{\bullet}Cl + CH_4$				
$\Delta E_{fwd}^{\ddagger}$	23.8	26.3	34.5	29.4	31.8	37.0	34.2	32.6
$\Delta E_{rev}^{\ddagger}$	−4.5	−3.3	12.2	1.9	7.6	9.7	10.9	7.2
ΔE	28.4	29.6	22.3	27.5	24.1	27.3	23.3	25.4
				$^{\bullet}Cl + CH_3NH_3^+$				
$\Delta E_{fwd}^{\ddagger}$	70.1	73.0	80.9	75.5	77.9	81.8	80.0	77.4
$\Delta E_{rev}^{\ddagger}$	25.0	25.3	38.0	29.8	33.2	34.1	35.3	32.2
ΔE	45.1	47.7	42.8	45.7	44.6	47.7	44.7	45.2
				$^{\bullet}Cl + CH_3CHO$				
$\Delta E_{fwd}^{\ddagger}$	10.3	16.8	56.7	20.2	19.2	29.2	23.9	24.3
$\Delta E_{rev}^{\ddagger}$	33.4	34.1	34.7	35.2	33.0	41.8	43.5	41.2
ΔE	−23.1	−17.2	22.0	−15.1	−13.8	−12.6	−19.6	−16.8
				$^{\bullet}Cl + CH_3COOH$				
$\Delta E_{fwd}^{\ddagger}$	20.8	26.7	38.4	27.8	27.2	35.9	35.2	32.5
$\Delta E_{rev}^{\ddagger}$	27.0	27.3	31.8	30.2	27.3	34.4	36.0	34.4
ΔE	−6.2	−0.7	6.6	−2.3	−0.1	1.5	−0.9	−1.9
				$^{\bullet}Cl + CH_3COO^-$				
$\Delta E_{fwd}^{\ddagger}$	−62.0	−49.6	−36.8	−52.1	−36.7	−41.6	−43.9	−43.8
$\Delta E_{rev}^{\ddagger}$	−54.2	−46.6	−32.5	−46.4	−33.3	−39.1	−35.5	−38.1
ΔE	−7.8	−3.0	−4.4	−5.7	−3.4	−2.5	−8.4	−5.7
				$^{\bullet}Cl + CH_3NH_2$				
$\Delta E_{fwd}^{\ddagger}$	−52.3	−38.1	−5.8	−33.9	−5.3	−14.8	−12.2	−15.5
$\Delta E_{rev}^{\ddagger}$	−21.2	−9.2	21.2	−5.4	20.1	7.8	12.0	10.9
ΔE	−31.1	−28.9	−27.0	−28.5	−25.5	−22.5	−24.2	−26.4
				MD[c]				
$\Delta E_{fwd}^{\ddagger}$	−10.4	−6.0	10.9	−3.5	−2.7	4.3	1.6	
$\Delta E_{rev}^{\ddagger}$	−8.5	−7.9	0.4	−4.5	−3.5	1.2	2.7	
ΔE	−2.4	1.3	7.1	0.3	1.0	3.2	−0.8	
				MAD[c]				
$\Delta E_{fwd}^{\ddagger}$	10.4	6.0	10.9	3.5	3.0	4.3	1.8	
$\Delta E_{rev}^{\ddagger}$	8.5	7.9	4.9	4.5	4.2	1.2	2.7	
ΔE	3.4	2.3	9.1	1.2	1.7	3.2	1.9	
overall	7.4	5.4	8.3	3.0	2.9	2.9	2.1	
				LD[c]				
$\Delta E_{fwd}^{\ddagger}$	−14.0	−7.5	32.4	−4.7	0.5	4.9	2.7	
$\Delta E_{rev}^{\ddagger}$	−11.8	−10.6	−6.5	−6.0	−8.2	2.5	3.7	
ΔE	−6.3	4.2	38.9	2.1	3.0	4.2	−2.8	

[a] All relative energies are vibrationless values, and each forward barrier, $\Delta E_{fwd}^{\ddagger}$, and reaction energy, ΔE, is corrected for the −3.52 kJ mol^{-1} $^{\bullet}Cl$ SO stabilization. [b] All geometries were optimized using the UQCISD/6-31+G(d,p) level of theory. [c] MD, MAD, and LD are mean deviation, mean absolute deviation, and largest deviation, respectively, from W1′ values. The "overall" MAD is an average for the MAD of the forward and reverse barriers and reaction energies. The "barriers" for the $^{\bullet}Cl + CH_3CO_2^-$ and $^{\bullet}Cl + CH_3NH_2$ reactions have been excluded from the statistics.

for reactions with increasing exothermicity. In each TS, the electronegative chlorine is negatively charged, and the extent of polarization is determined by the electron-donating (or -withdrawing) ability of the substituent. The most stabilized TSs occur in the $^{\bullet}Cl + CH_3CO_2^-$ and $^{\bullet}Cl + CH_3NH_2$ reactions, as the CO_2^- and NH_2 groups contribute to low-lying charge-transfer configurations as well as to stable product radicals. The least stabilized TS occurs in the $^{\bullet}Cl + CH_3NH_3^+$ reaction, due to the destabilizing interaction between the positive end of the incipient HCl dipole and the positively charged $^{\bullet}CH_2NH_3^+$ group. The salience of TS polarization in determining H-abstraction barrier heights is consistent with the experimental findings of Easton and co-workers for analogous larger systems[8] and is currently the subject of further investigation.

The second goal of the present study was to benchmark the performance of a range of electronic structure methods that are less computationally demanding than W1′. Our findings may be summarized as follows.

(1) The sensitivity of the calculated geometries to the level of theory used for geometry optimization was assessed by comparing $^{\bullet}Cl + CH_4$ TS geometries with a UCCSD(T)/6-311+G(3df,2p)-optimized TS as the benchmark, while TSs for the remaining five reactions were compared with UQCISD/6-31+G(d,p)-optimized TSs as the benchmarks. For the $^{\bullet}Cl + CH_4$ TS, UQCISD/6-31+G(d,p) optimization yields a structure in which r_{Cl-H}, r_{H-C}, and r_{Cl-C} all agree with the benchmark to within 0.004 Å. This close agreement suggests that optimizations at the UQCISD/6-31+G(d,p) level provide an appropriate benchmark for the remaining five reactions. Across the four reactions possessing barriers to H-abstraction, UHF/6-31+G(d,p) optimizations produce r_{Cl-H}, r_{H-C}, and r_{Cl-C} values that agree with the benchmark values to within ∼5%. The hybrid DFT methods, UBMK and UB3-LYP/6-

31+G(d,p), perform least well for the $^{\bullet}Cl + CH_4$ reaction, overestimating the benchmark r_{H-C} value by 6−18%, while performing comparably well to UHF/6-31+G(d,p) for the remaining five reactions.

(2) The variation in barrier heights and reaction energies with geometry was assessed by carrying out UCCSD(T)/6-311+G(3df,2p) single-point energy calculations on the reactant, TS, and product geometries optimized using a range of methods. For the $^{\bullet}Cl + CH_4$ reaction, UQCISD/6-31+G(d,p)-optimized geometries provide $\Delta E_{fwd}^{\ddagger}$, $\Delta E_{rev}^{\ddagger}$, and ΔE values that lie within 0.1 kJ mol^{-1} of the benchmarks, provided by UCCSD(T)/6-311+G(3df,2p) geometries. For the four reactions with barriers to H-abstraction, namely, $^{\bullet}Cl + CH_4$, $^{\bullet}Cl + CH_3NH_3^+$, $^{\bullet}Cl + CH_3CHO$, and $^{\bullet}Cl + CH_3CO_2H$, UHF/6-31+G(d,p)-optimized geometries result in $\Delta E_{fwd}^{\ddagger}$, $\Delta E_{rev}^{\ddagger}$, and ΔE values that agree to within 0.8 kJ mol^{-1} of the benchmark, while UB3-LYP/6-31+G(d,p)-optimized geometries result in $\Delta E_{fwd}^{\ddagger}$, $\Delta E_{rev}^{\ddagger}$, and ΔE values that agree to within 3.5 kJ mol^{-1} of the benchmark. Both the UBMK and the UB3-LYP/6-31+G(d,p)-optimized geometries show slightly poorer performance for the $^{\bullet}Cl + CH_4$ reaction, producing $\Delta E_{fwd}^{\ddagger}$ and $\Delta E_{rev}^{\ddagger}$ values that underestimate the benchmark by up to 4.0 kJ mol^{-1}.

(3) The performance of a range of methods for calculating barrier heights and reaction energies, using reactant, TS, and product geometries optimized uniformly at the UQCISD/6-31+G(d,p) level of theory was examined. We recommend the G3X(MP2)-RAD procedure as a secondary benchmark for cases in which W1′ is too expensive, as it produces barriers and reaction energies with MAD < 3 kJ mol^{-1}, when compared with W1′. For cases in which the G3X(MP2)-RAD procedure is too expensive, we recommend RMP2/G3XLarge, as it provides reaction energetics of comparable accuracy to those from UCCSD(T)/G3XLarge calculations. While RMP2/G3XLarge was shown to provide accurate barriers and reaction energies, we found that RMP2/6-31+G(d,p) calculations overestimated each of the forward barriers and reaction energies by 20−40 kJ mol^{-1}, with respect to the benchmarks. Care must be taken with UMP2 calculations of barriers and reaction energies, because spin contamination in the TS and product radical wave functions, found for two of the six reactions, leads to a significant overestimation in the barriers and reaction energy. Finally, when the hybrid and double-hybrid DFT methods are considered, the accuracy of the computed barriers and reaction energies, when compared with the W1′ values, improves from UB3-LYP to UBMK to UB2-PLYP. The accuracy of the UB2-PLYP/G3XLarge barriers and reaction energies is comparable with that of the RMP2/G3XLarge values, and thus, UB2-PLYP/G3XLarge is recommended as an additional reliable method.

Acknowledgment. We gratefully acknowledge funding (to C.J.E. and L.R.) from Australian Research Council Discovery Grants and from the ARC Centre of Excellence for Free Radical Chemistry and Biotechnology and generous allocations of computing time (to L.R.) from the National Computational Infrastructure (NCI) National Facility and the Australian Centre for Advanced Computing and Communication (ac3).

Supporting Information Available: GAUSSIAN 03 archive entries for UQCISD/6-31+G(d,p)-optimized geometries of relevant equilibrium structures and TSs (Table S1) and calculated W1′//UQCISD/6-31+G(d,p) total energies (Table S2). This material is available free of charge via the Internet at http://pubs.acs.org.

References and Notes

(1) Wayne, R. P. *Chemistry of Atmospheres*, 3rd ed.; Oxford University Press: Oxford, 2000.

(2) (a) Platt, U.; Honninger, G. *Chemosphere* **2003**, *52*, 325. (b) Finlayson-Pitts, B. J. *Chem. Rev.* **2003**, *103*, 4801. (c) Tanaka, P. L.; Riemer, D. D.; Chang, S.; Yarwood, G.; McDonald-Buller, E. C.; Apel, E. C.; Orlando, J. J.; Silva, P. J.; Jimenez, J. L.; Canagaratna, M. R.; Neece, J. D.; Mullins, C. B.; Allen, D. T. *Atmos. Environ.* **2003**, *37*, 1393. (d) Knipping, E. M.; Dabdub, D. *Environ. Sci. Technol.* **2003**, *37*, 275.

(3) (a) Gullett, B. K.; Sarofim, A. F.; Smith, K. A.; Procaccini, C. *Process Saf. Environ. Prot.* **2000**, *78*, 47. (b) Babushok, V. I.; Tsang, W. *Chemosphere* **2003**, *51*, 1023. (c) Procaccini, C.; Bozzelli, J. W.; Longwell, J. P.; Sarofim, A. F.; Smith, K. A. *Environ. Sci. Technol.* **2003**, *37*, 1684. (d) Stanmore, B. R. *Combust. Flame* **2004**, *136*, 398.

(4) (a) Gilbert, B. C.; Stell, J. K.; Peet, W. J.; Radford, K. J. *J. Chem. Soc., Faraday Trans. 1* **1988**, *84*, 3319. (b) Nelson, L.; Rattigan, O.; Neavyn, R.; Sidebottom, H.; Treacy, J. *Int. J. Chem. Kinet.* **1990**, *22*, 1111. (c) Tuazon, E. C.; Atkinson, R.; Corchnoy, S. B. *Int. J. Chem. Kinet.* **1992**, *24*, 639. (d) Jacobi, H. W.; Herrmann, H.; Zellner, R. *Ber. Bunsen-Ges. Phys. Chem.* **1997**, *101*, 1909. (e) Sevilla, M. D.; Summerfield, S.; Eliezer, I.; Rak, J.; Symons, M. C. R. *J. Phys. Chem. A* **1997**, *101*, 2910. (f) Notario, A.; Le Bras, G.; Mellouki, A. *J. Phys. Chem. A* **1998**, *102*, 3112. (g) Buxton, G. V.; Bydder, M.; Salmon, G. A. *J. Chem. Soc., Faraday Trans.* **1998**, *94*, 653. (h) Crim, F. F. *Acc. Chem. Res.* **1999**, *32*, 877. (i) Buxton, G. V.; Bydder, M.; Salmon, G. A. *Phys. Chem. Chem. Phys.* **1999**, *1*, 269. (j) Buxton, G. V.; Wang, J.; Salmon, G. A. *Phys. Chem. Chem. Phys.* **2001**, *3*, 2618. (k) Martire, D. O.; Rosso, J. A.; Bertolotti, S.; Le Roux, G. C.; Braun, A. M.; Gonzalez, M. C. *J. Phys. Chem. A* **2001**, *105*, 5385. (l) Rudic, S.; Murray, C.; Ascenzi, D.; Anderson, H.; Harvey, J. N.; Orr-Ewing, A. J. *J. Chem. Phys.* **2002**, *117*, 5692. (m) Wicktor, F.; Donati, A.; Herrmann, H.; Zellner, R. *Phys. Chem. Chem. Phys.* **2003**, *5*, 2562. (n) Herrmann, H. *Chem. Rev.* **2003**, *103*, 4691. (o) Murray, C.; Retail, B.; Orr-Ewing, A. *J. Chem. Phys.* **2004**, *301*, 239. (p) Yu, X.-Y.; Bao, Z.-C.; Barker, J. R. *J. Phys. Chem. A* **2004**, *108*, 295. (q) Murray, C.; Orr-Ewing, A. J. *Int. Rev. Phys. Chem.* **2004**, *23*, 435. (r) Zhu, L.; Nicovich, J. M.; Wine, P. H. *J. Phys. Chem. A* **2005**, *109*, 3903. (s) Kim, Z. H.; Bechtel, H. A.; Camden, J. P.; Zare, R. N. *J. Chem. Phys.* **2005**, *122*, 084303. (t) Murray, C.; Pearce, J. K.; Rudic, S.; Retail, B.; Orr-Ewing, A. J. *J. Phys. Chem. A* **2005**, *109*, 11093. (u) Camden, J. P.; Bechtel, H. A.; Brown, D. J. A.; Zare, R. N. *J. Chem. Phys.* **2006**, *124*, 034311. (v) Elles, C. G.; Crim, F. F. *Annu. Rev. Phys. Chem.* **2006**, *57*, 273. (w) Holiday, R. J.; Kwon, C. H.; Annesley, C. J.; Crim, F. F. *J. Chem. Phys.* **2006**, *125*, 133101. (x) Sheps, L.; Crowther, A. C.; Carrier, S. L.; Crim, F. F. *J. Phys. Chem. A* **2006**, *110*, 3087. (y) Martin, M. R.; Brown, D. J. A.; Chiou, A. S.; Zare, R. N. *J. Chem. Phys.* **2007**, *126*, 044315. (z) Pearce, J. K.; Retail, B.; Greaves, S. J.; Rose, R. A.; Orr-Ewing, A. J. *J. Phys. Chem. A* **2007**, *111*, 13296.

(5) (a) Easton, C. J. *Chem. Rev.* **1997**, *97*, 53. (b) Robertson, J.; Pillai, J.; Lush, R. K. *Chem. Soc. Rev.* **2001**, *30*, 94. (c) Hansen, S. G.; Skrydstrup, T. *Top. Curr. Chem.* **2006**, *264*, 135. (d) Albert, M.; Fensterbank, L., Lacôte, E.; Malacria, M. In *Radicals in Synthesis II*; Gansäuer, A., Ed.; Springer: Heidelberg, 2006; Vol. 264; pp 1−62. (e) Zimmerman, J.; Sibi, M. P. In *Radicals in Synthesis I*; Gansäuer, A., Ed.; Springer: Heidelberg, 2006; Vol. 263, pp 107−162.

(6) (a) Stubbe, J.; van der Donk, W. A. *Chem. Rev.* **1998**, *98*, 705. (b) Licht, S.; Stubbe, J. In *Comprehensive Natural Products Chemistry*; Barton, D. H. R., Nakanishi, K., Meth-Cohn, O., Eds.; Elsevier Science B.V.: Amsterdam, 1999; Vol. 5, pp 163−203. (c) Bogdan, C.; Röllinghoff, M.; Diefenbach, A. *Curr. Opin. Immunol.* **2000**, *12*, 64. (d) Gruber, K.; Kratky, C. *Curr. Opin. Chem. Biol.* **2002**, *6*, 598. (e) Banerjee, R. *Chem. Rev.* **2003**, *103*, 2083. (f) Stubbe, J.; Nocera, D. G.; Yee, C. S.; Chang, M. C. Y. *Chem. Rev.* **2003**, *103*, 2167. (g) Himo, F.; Siegbahn, P. E. M. *Chem. Rev.* **2003**, *103*, 2421. (h) Toraya, T. *Chem. Rev.* **2003**, *103*, 2095. (i) Frey, P. A.; Hegeman, A. D.; Reed, G. H. *Chem. Rev.* **2006**, *106*, 3302. (j) Lambeth, J. D. *Nat. Rev. Immunol.* **2004**, *4*, 181. (k) Reece, S. Y.; Hodgkiss, J. M.; Stubbe, J.; Nocera, D. G. *Philos. Trans. R. Soc. London, Ser. B* **2006**, *361*, 1351.

(7) (a) Davies, M. J.; Dean, R. T. *Radical-Mediated Protein Oxidation: From Chemistry to Medicine*; Oxford University Press: New York, 1997. (b) Dean, R. T.; Fu, S.; Stocker, R.; Davies, M. J. *Biochem. J.* **1997**, *324*, 1. (c) Fu, S.; Davies, M. J.; Dean, R. T. In *Molecular Biology of Free Radicals in Human Diseases*; Aruoma, O. I., Halliwell, B., Eds.; OICA International: London, 1998; pp 29−56. (d) Burkitt, M. J. In *Electron Paramagnetic Resonance*; Gilbert, B. C., Davies, M. J., Murphy, D. M., Eds.; The Royal Society of Chemistry: Cambridge, 2002; Vol. 18, pp 1−46. (e) Ostdal, H.; Davies, M. J.; Andersen, H. J. *Free Radical Biol. Med.* **2002**, *33*, 201. (f) Hussain, S. P.; Hofseth, L. J.; Harris, C. C. *Nat. Rev. Cancer* **2003**, *3*, 276. (g) Finkel, T. *Nat. Rev. Mol. Cell Biol.* **2005**, *6*, 971. (h) Davies, M. J. *Biochim. Biophys. Acta, Proteins Proteomics* **2005**, *1703*, 93. (i) Federico, A.; Morgillo, F.; Tuceillo, C.; Ciardiello, F.; Loguercio, C. *Int. J. Cancer* **2007**, *121*, 2381. (j) Lipton, S. A.; Gu, Z.; Nakamura, T. In *International Review of Neurobiology*; Bradley, R., Harris, A. P. J., Eds.; Elsevier: Amsterdam, 2007; Vol. 82, pp 1−27.

(8) Watts, Z.; Easton, C. J. Unpublished data. For an earlier qualitative study, see Kollonitsch, J.; Scott, A. N.; Doldouras, G. A. *J. Am. Chem. Soc.* **1966**, *88*, 3624.

(9) Martin, J. M. L. *Chem. Phys. Lett.* **1999**, *310*, 271.

(10) Martin, J. M. L.; de Oliveira, G. *J. Chem. Phys.* **1999**, *111*, 1843.

(11) Parthiban, S.; Martin, J. M. L. *J. Chem. Phys.* **2001**, *114*, 6014.

(12) Parthiban, S.; Martin, J. M. L. In *Quantum-Mechanical Prediction of Thermochemical Data*; Cioslowski, J., Ed.; Kluwer Academic Publishers: Dordrecht, 2001; pp 31−65.

(13) Hehre, W. J.; Radom, L.; Schleyer, P. v. R.; Pople, J. A. *Ab Initio Molecular Orbital Theory*; Wiley: New York, 1986.

(14) Jensen, F. *Introduction to Computational Chemistry*, 2nd ed.; Wiley: Chichester, 2006.

(15) Koch, W.; Holthausen, M. C. *A Chemist's Guide to Density Functional Theory*, 2nd ed.; Wiley-VCH: New York, 2001.

(16) Frisch, M. J.; Trucks, G. W.; Schlegel, H. B.; Scuseria, G. E.; Robb, M. A.; Cheeseman, J. R.; Montgomery, J. J. A.; Vreven, T.; Kudin, K. N.; Burant, J. C.; Millam, J. M.; Iyengar, S. S.; Tomasi, J.; Barone, V.; Mennucci, B.; Cossi, M.; Scalmani, G.; Rega, N.; Petersson, G. A.; Nakatsuji, H.; Hada, M.; Ehara, M.; Toyota, K.; Fukuda, R.; Hasegawa, J.; Ishida, M.; Nakajima, T.; Honda, Y.; Kitao, O.; Nakai, H.; Klene, M.; Li, X.; Knox, J. E.; Hratchian, H. P.; Cross, J. B.; Bakken, V.; Adamo, C.; Jaramillo, J.; Gomperts, R.; Stratmann, R. E.; Yazyev, O.; Austin, A. J.; Cammi, R.; Pomelli, C.; Ochterski, J. W.; Ayala, P. Y.; Morokuma, K.; Voth, G. A.; Salvador, P.; Dannenberg, J. J.; Zakrzewski, V. G.; Dapprich, S.; Daniels, A. D.; Strain, M. C.; Farkas, O.; Malick, D. K.; Rabuck, A. D.; Raghavachari, K.; Foresman, J. B.; Ortiz, J. V.; Cui, Q.; Baboul, A. G.; Clifford, S.; Cioslowski, J.; Stefanov, B. B.; Liu, G.; Liashenko, A.; Piskorz, P.; Komaromi, I.; Martin, R. L.; Fox, D. J.; Keith, T.; Al-Laham, M. A.; Peng, C. Y.; Nanayakkara, A.; Challacombe, M.; Gill, P. M. W.; Johnson, B.; Chen, W.; Wong, M. W.; Gonzalez, C.; Pople, J. A. *Gaussian*; Gaussian, Inc.: Wallingford, CT, 2004.

(17) Amos, R. D.; Bernhardsson, A.; Berning, A.; Celani, P.; Cooper, D. L.; Deegan, M. J. O.; Dobbyn, A. J.; Eckert, F.; Hampel, C.; Hetzer, G.; Knowles, P. J.; Korona, T.; Lindh, R.; Lloyd, A. W.; McNicholas, S. J.; Manby, F. R.; Meyer, W.; Mura, M. E.; Nicklass, A.; Palmieri, P.; Pitzer, R.; Rauhut, G.; Schütz, M.; Schumann, U.; Stoll, H.; Stone, A. J.; Tarroni, R.; Thorsteinsson, T.; Werner, H.-J. *MOLPRO*, version 2002.6; University of Birmingham: Birmingham, 2002.

(18) Werner, H.-J.; Knowles, P. J.; Lindh, R.; Manby, F. R.; Schütz, M.; Celani, P.; Korona, T.; Rauhut, G.; Amos, R. D.; Bernhardsson, A.; Berning, A.; Cooper, D. L.; Deegan, M. J. O.; Dobbyn, A. J.; Eckert, F.; Hampel, C.; Hetzer, G.; Lloyd, A. W.; McNicholas, S. J.; Meyer, W.; Mura, M. E.; Nicklass, A.; Palmieri, P.; Pitzer, R.; Schumann, U.; Stoll, H.; Stone, A. J.; Tarroni, R.; Thorsteinsson, T. *MOLPRO*, version 2006.1; University of Birmingham: Birmingham, 2006.

(19) Stanton, J. F.; Gauss, J.; Watts, J. D.; Nooijen, M.; Oliphant, N.; Perera, S. A.; Szalay, P. G.; Lauderdale, W. J.; Kucharski, S. A.; Gwaltney, S. R.; Beck, S.; Balkov, A.; Bernholdt, D. E.; Baeck, K. K.; Rozyczko, P.; Sekino, H.; Hober, C.; Bartlett, R. J. *ACES II*; University of Florida: Gainsville, FL, 1992.

(20) Merrick, J. P.; Moran, D.; Radom, L. *J. Phys. Chem. A* **2007**, *111*, 11683.

(21) Boese, A. D.; Oren, M.; Atasoylu, O.; Martin, J. M. L.; Kallay, M.; Gauss, J. *J. Chem. Phys.* **2004**, *120*, 4129.

(22) Karton, A.; Rabinovich, E.; Martin, J. M. L.; Ruscic, B. *J. Chem. Phys.* **2006**, *125*, 144108.

(23) Cowan, R. D.; Griffin, M. J. *J. Opt. Soc. Am.* **1976**, *66*, 1010.

(24) Gdanitz, R. J.; Ahlrichs, R. *Chem. Phys. Lett.* **1988**, *143*, 413.

(25) Uehara, H.; Horiai, K. *J. Opt. Soc. Am. B* **1987**, *4*, 1217.

(26) (a) Foster, J. P.; Weinhold, F. *J. Am. Chem. Soc.* **1980**, *102*, 7211. (b) Reed, A. E.; Weinhold, F. *J. Chem. Phys.* **1983**, *78*, 4066. (c) Reed, A. E.; Weinstock, R. B.; Weinhold, F. *J. Chem. Phys.* **1985**, *83*, 735. (d) Reed, A. E.; Weinhold, F. *J. Chem. Phys.* **1985**, *83*, 1736. (e) Carpenter, J. E.; Weinhold, F. *THEOCHEM* **1988**, *46*, 41. (f) Reed, A. E.; Curtiss, L. A.; Weinhold, F. *Chem. Rev.* **1988**, *88*, 899. (g) Carpenter, J. E.; Weinhold, F. *J. Am. Chem. Soc.* **1988**, *110*, 368.

(27) Beare, K. D.; Coote, M. L. *J. Phys. Chem. A* **2004**, *108*, 7211.

(28) Henry, D. J.; Sullivan, M. B.; Radom, L. *J. Chem. Phys.* **2003**, *118*, 4849.

(29) Grimme, S. *J. Chem. Phys.* **2006**, *124*, 034108.

(30) Curtiss, L. A.; Redfern, P. C.; Raghavachari, K.; Pople, J. A. *J. Chem. Phys.* **2001**, *114*, 108.

(31) Malick, D. K.; Petersson, G. A.; Montgomery, J. A., Jr. *J. Chem. Phys.* **1998**, *108*, 5704.

(32) Linstrom, P. J.; Mallard, W. G., Eds. *NIST Chemistry WebBook, NIST Standard Reference Database Number 69*; National Institute of Standards and Technology: Gaithersburg, MD, June, 2005.

(33) Wang, X. B.; Woo, H. K.; Wang, L. S.; Minofar, B.; Jungwirth, P. *J. Phys. Chem. A* **2006**, *110*, 5047.

(34) Parkinson, C. J.; Mayer, P. M.; Radom, L. *J. Chem. Soc., Perkin Trans. 2* **1999**, *11*, 2305.

(35) (a) Henry, D. J.; Parkinson, C. J.; Mayer, P. M.; Radom, L. *J. Phys. Chem. A* **2001**, *105*, 6750. (b) Menon, A. S.; Wood, G. P. F.; Moran, D.; Radom, L. *J. Phys. Chem. A* **2007**, *111*, 13638.

(36) Zipse, H. *Top. Curr. Chem.* **2006**, *263*, 163.

(37) (a) Pasto, D. J.; Krasnansky, R.; Zercher, C. *J. Org. Chem.* **1987**, *52*, 3062. (b) Song, K.-S.; Liu, L.; Guo, Q.-X. *J. Org. Chem.* **2003**, *68*, 4604.

(38) (a) Pross, A.; Yamataka, H.; Nagase, S. *J. Phys. Org. Chem.* **1991**, *4*, 135. (b) Salikhov, A.; Fischer, H. *Theor. Chem. Acc.* **1997**, *96*, 114. (c) Donahue, N. M.; Clarke, J. S.; Anderson, J. G. *J. Phys. Chem. A* **1998**, *102*, 3923.

(39) (a) Pross, A. *Adv. Phys. Org. Chem.* **1985**, *21*, 99. (b) Yamataka, H.; Nagase, S. *J. Org. Chem.* **1988**, *53*, 3232. (c) Shaik, S.; Hiberty, P. C. *Adv. Quantum Chem.* **1995**, *26*, 99. (d) Zavitsas, A. A.; Chatgilialoglu, C. *J. Am. Chem. Soc.* **1995**, *117*, 10645. (e) Bernardi, F.; Bottoni, A. *J. Phys. Chem. A* **1997**, *101*, 1912. (f) Pais, A. A. C. C.; Arnaut, L. G.; Formosinho, S. J. *J. Chem. Soc., Perkin Trans. 2* **1998**, 2577. (g) Zavitsas, A. A. *J. Am. Chem. Soc.* **1998**, *120*, 6578. (h) Shaik, S.; Shurki, A. *Angew. Chem., Int. Ed.* **1999**, *38*, 586. (i) Clarke, J. S.; Rypkema, H. A.; Kroll, J. H.; Donahue, N. M.; Anderson, J. G. *J. Phys. Chem. A* **2000**, *104*, 4458. (j) Shaik, S.; Wu, W.; Dong, K.; Song, L.; Hiberty, P. C. *J. Phys. Chem. A* **2001**, *105*, 8226. (k) Shaik, S.; Wu, W.; Dong, K.; Song, L.; Hiberty, P. C. *J. Phys. Chem. A* **2001**, *105*, 8226. (l) Rypkema, H. A.; Donahue, N. M.; Anderson, J. G. *J. Phys. Chem. A* **2001**, *105*, 1498. (m) Zavitsas, A. A. *J. Phys. Chem. A* **2002**, *106*, 5041. (n) Shaik, S.; de Visser, S. P.; Wu, W.; Song, L.; Hiberty, P. C. *J. Phys. Chem. A* **2002**, *106*, 5043. (o) Song, L.; Wu, W.; Dong, K.; Hiberty, P. C.; Shaik, S. *J. Phys. Chem. A* **2002**, *106*, 11361. (p) Song, L.; Wu, W.; Hiberty, P. C.; Danovich, D.; Shaik, S. *Chem.—Eur. J.* **2003**, *9*, 4540. (q) Su, P.; Song, L.; Wu, W.; Hiberty, P. C.; Shaik, S. *J. Am. Chem. Soc.* **2004**, *126*, 13539. (r) Shaik, S.; Hiberty, P. C. In *Theory and Applications of Computational Chemistry: The First Forty Years*; Dykstra, C. E., Frenking, G., Kim, K. S., Scuseria, G. E., Eds.; Elsevier: Amsterdam, 2005; pp 635−668. (s) Hiberty, P. C.; Megret, C.; Song, L.; Wu, W.; Shaik, S. *J. Am. Chem. Soc.* **2006**, *128*, 2836. (t) Hiberty, P. C.; Shaik, S. *J. Comput. Chem.* **2007**, *28*, 137.

(40) (a) Simpson, W. R.; Orr-Ewing, A. J.; Zare, R. N. *Chem. Phys. Lett.* **1993**, *212*, 163. (b) Saueressig, G.; Bergamaschi, P.; Crowley, J. N.; Fischer, H.; Harris, G. W. *Geophys. Res. Lett.* **1995**, *22*, 1225. (c) Saueressig, G.; Bergamaschi, P.; Crowley, J. N.; Fischer, H.; Harris, G. W. *Geophys. Res. Lett.* **1996**, *23*, 3619. (d) Bergamaschi, P.; Brühl, C.; Brenninkmeijer, C. A. M.; Saueressig, G.; Crowley, J. N.; Grooss, J. U.; Fischer, H.; Crutzen, P. J. *Geophys. Res. Lett.* **1996**, *23*, 2227. (e) Seeley, J. V.; Jayne, J. T.; Molina, M. J. *J. Phys. Chem.* **1996**, *100*, 4019. (f) Simpson, W. R.; Rakitzis, T. P.; Kandel, S. A.; Lev-On, T.; Zare, R. N. *J. Phys. Chem.* **1996**, *100*, 7938. (g) Pilgrim, J. S.; McIlroy, A.; Taatjes, C. A. *J. Phys. Chem. A* **1997**, *101*, 1873. (h) Gupta, M. L.; McGrath, M. P.; Cicerone, R. J.; Rowland, F. S.; Wolfsberg, M. *Geophys. Res. Lett.* **1997**, *24*, 2761. (i) Kandel, S. A.; Zare, R. N. *J. Chem. Phys.* **1998**, *109*, 9719. (j) Wang, J. J.; Keyser, L. F. *J. Phys. Chem. A* **1999**, *103*, 7460. (k) Crowley, J. N.; Saueressig, G.; Bergamaschi, P.; Fischer, H.; Harris, G. W. *Chem. Phys. Lett.* **1999**, *303*, 268. (l) Tyler, S. C.; Ajie, H. O.; Rice, A. L.; Cicerone, R. J.; Tuazon, E. C. *Geophys. Res. Lett.* **2000**, *27*, 1715. (m) Boone, G. D.; Agyin, F.; Robichaud, D. J.; Tao, F.-M.; Hewitt, S. A. *J. Phys. Chem. A* **2001**, *105*, 1456. (n) Kim, Z. H.; Alexander, A. J.; Bechtel, H. A.; Zare, R. N. *J. Chem. Phys.* **2001**, *115*, 179. (o) Michelsen, H. A.; Simpson, W. R. *J. Phys. Chem. A* **2001**, *105*, 1476. (p) Michelsen, H. A. *J. Geophys. Res. Atmos.* **2001**, *106*, 12267. (q) Bryukov, M. G.; Slagle, I. R.; Knyazev, V. D. *J. Phys. Chem. A* **2002**, *106*, 10532. (r) Yoon, S.; Henton, S.; Zivkovic, A. N.; Crim, F. F. *J. Chem. Phys.* **2002**, *116*, 10744. (s) Bechtel, H. A.; Camden, J. P.; Brown, D. J. A.; Zare, R. N. *J. Chem. Phys.* **2004**, *120*, 5096. (t) Bechtel, H. A.; Camden, J. P.; Brown, D. J. A.; Martin, M. R.; Zare, R. N.; Vodopyanov, K. *Angew. Chem., Int. Ed.* **2005**, *44*, 2382. (u) Zhou, J.; Zhang, B.; Lin, J. J.; Liu, K. *Mol. Phys.* **2005**, *103*, 1757. (v) Sellevg, S. R.; Nyman, G.; Nielsen, C. J. *J. Phys. Chem. A* **2006**, *110*, 141.

(41) (a) Truong, T. N.; Truhlar, D. G.; Baldridge, K. K.; Gordon, M. S.; Steckler, R. *J. Chem. Phys.* **1989**, *90*, 7137. (b) Chen, Y.; Tschuikow-Roux, E.; Rauk, A. *J. Phys. Chem.* **1991**, *95*, 9832. (c) Dobbs, K. D.; Dixon, D. A. *J. Phys. Chem.* **1994**, *98*, 12584. (d) Wang, X.; Ben-Nun, M.; Levine, R. D. *Chem. Phys.* **1995**, *197*, 1. (e) Duncan, W. T.; Truong, T. N. *J. Chem. Phys.* **1995**, *103*, 9642. (f) Espinosa-Garcia, J.; Corchado, J. C. *J. Chem. Phys.* **1996**, *105*, 3517. (g) Tanaka, N.; Xiao, Y.; Lasaga, A. C. *J. Atmos. Chem.* **1996**, *23*, 37. (h) Nyman, G.; Yu, H.-G.; Walker, R. B. *J. Chem. Phys.* **1998**, *109*, 5896. (i) Roberto-Neto, O.; Coitino, E. L.; Truhlar, D. G. *J. Phys. Chem. A* **1998**, *102*, 4568. (j) Yu, H.-G.; Nyman, G. *J. Chem. Phys.* **1999**, *110*, 7233. (k) Yu, H.-G.; Nyman, G. *J. Chem. Phys.* **1999**, *111*, 6693. (l) Yu, H.-G.; Nyman, G. *Phys. Chem. Chem. Phys.* **1999**, *1*, 1181. (m) Corchado, J. C.; Truhlar, D. G.; Espinosa-Garcia, J. *J. Chem. Phys.* **2000**, *112*, 9375. (n) Skokov, S.; Bowman, J. M. *J. Chem. Phys.* **2000**, *113*, 4495. (o) Zhou, Z.; Chen, G.; Zhou, X.; Fu, H. *Int. J. Quantum Chem.* **2002**, *87*, 49. (p) Garcia, E.; Sanchez, C.; Saracibar, A.; Lagana, A. *J. Phys. Chem. A* **2004**, *108*, 8752. (q) Rangel, C.; Espinosa-Garcia, J.; Corchado, J. C. *J. Phys. Chem. A* **2005**, *109*, 8071. (r) Garcia, E.; Sanchez, C.; Rodriguez, A.; Lagana, A. *Int. J. Quantum Chem.* **2005**, *106*, 623. (s)

Varandas, A. J. C.; Caridade, P. J. S. B.; Zhang, J. Z. H.; Cui, Q.; Han, K. L. *J. Chem. Phys.* **2006**, *125*, 064312. (t) Troya, D.; Weiss, P. J. E. *J. Chem. Phys.* **2006**, *124*, 074313. (u) Sanson, J.; Corchado, J. C.; Rangel, C.; Espinosa-Garcia, J. *J. Phys. Chem. A* **2006**, *110*, 9568. (v) Banks, S. T.; Clary, D. C. *Phys. Chem. Chem. Phys.* **2007**, *9*, 933.

(42) (a) Troya, D.; Millan, J.; Banos, I.; Gonzalez, M. *J. Chem. Phys.* **2002**, *117*, 5730. (b) Castillo, J. F.; Aoiz, F. J.; Banares, L. *J. Chem. Phys.* **2006**, *125*, 124316. (c) Rangel, C.; Navarrete, M.; Corchado, J. C.; Espinosa-Garcia, J. *J. Chem. Phys.* **2006**, *124*, 124306.

(43) See, for example, Lynch, B. J.; Truhlar, D. G. *J. Phys. Chem. A* **2001**, *105*, 2936.

(44) The experimental vibrationless reaction energy, ΔE_{exp}, was calculated from the experimental[45] $\Delta_f H°$ (0 K) of $^{\bullet}Cl$, CH_4, HCl, and $^{\bullet}CH_3$, by subtracting the experimental[46] or calculated[47] zero-point vibrational energies, the latter of which were corrected using the method of Martin et al.[22]

(45) (a) Ruscic, B.; Pinzon, R. E.; Morton, M. L.; von Laszevski, G.; Bittner, S. J.; Nijsure, S. G.; Amin, K. A.; Minkoff, M.; Wagner, A. F. *J. Phys. Chem. A* **2004**, *108*, 9979. (b) Ruscic, B.; Boggs, J. E.; Burcat, A.; Csaszar, A. G.; Demaison, J.; Janoschek, R.; Martin, J. M. L.; Morton, M. L.; Rossi, M. J.; Stanton, J. F.; Szalay, P. G.; Westmoreland, P. R.; Zabel, F.; Berces, T. *J. Phys. Chem. Ref. Data* **2005**, *34*, 573.

(46) Irikura, K. K. *J. Phys. Chem. Ref. Data* **2007**, *36*, 389.

(47) (a) Schwenke, D. W. *Spectrochim. Acta* **1999**, *55A*, 731. (b) Schwenke, D. W. *Spectrochim. Acta* **2002**, *58A*, 849.

(48) See, for example: (a) Cohen, A. J.; Mori-Sanchez, P.; Yang, W. *J. Chem. Phys.* **2007**, *126*, 191109. (b) Johansson, A. J.; Blomberg, M. R. A.; Siegbahn, P. E. M. *J. Chem. Phys.* **2008**, *129*, 154301. (c) Schwabe, T.; Grimme, S. *Eur. J. Org. Chem.* **2008**, 5928.

(49) Eskola, A. J.; Seetula, J. A.; Timonen, R. S. *Chem. Phys.* **2006**, *331*, 26.

(50) The experimental reaction enthalpy, ΔH_{rxn} (298 K), was calculated from the experimental $\Delta_f H°$ (298 K) of $^{\bullet}Cl$ and HCl,[45] CH_3NH_2, and $^{\bullet}CH_2NH_2$[51] and the experimental proton affinities of CH_3NH_2 and $^{\bullet}CH_2NH_2$.[52] The experimental reaction energy, ΔE_{exp}, was calculated from ΔH_{rxn} (298 K) by subtracting the scaled QCISD/6-31+G(d,p) thermal corrections and zero-point vibrational energies. [53]

(51) (a) Burkey, T. J.; Castelhano, A. L.; Griller, D.; Lossing, F. P. *J. Am. Chem. Soc.* **1983**, *105*, 4701. (b) Bodi, A.; Kercher, J. P.; Bond, C.; Meteesatien, P.; Sztaray, B.; Baer, T. *J. Phys. Chem. A* **2006**, *110*, 13425.

(52) Hunter, E. P. L.; Lias, S. G. *J. Phys. Chem. Ref. Data* **1998**, *27*, 413.

(53) Nicolaides, A.; Rauk, A.; Glukhovtsev, M. N.; Radom, L. *J. Phys. Chem.* **1996**, *100*, 17460.

(54) In cases such as this situation, where interconversion among the various reactant complexes and/or product complexes has not been fully characterized, we have enclosed the relevant part of the potential energy profile in a dashed box.

(55) (a) Niki, H.; Maker, P. D.; Savage, C. M.; Breitenbach, L. P. *J. Phys. Chem.* **1985**, *89*, 588. (b) Payne, W. A.; Nava, D. F.; Nesbitt, F. L.; Stief, L. J. *J. Phys. Chem.* **1990**, *94*, 7190. (c) Tyndall, G. S.; Orlando, J. J.; Kegley-Owen, C. S.; Wallington, T. J.; Hurley, M. D. *Int. J. Chem. Kinet.* **1999**, *31*, 776. (d) Kegley-Owen, C. S.; Tyndall, G. S.; Orlando, J. J.; Fried, A. *Int. J. Chem. Kinet.* **1999**, *31*, 766. (e) Smith, J. D.; DeSain, J. D.; Taatjes, C. A. *Chem. Phys. Lett.* **2002**, *366*, 417. (f) Seakins, P. W.; Orlando, J. J.; Tyndall, G. S. *Phys. Chem. Chem. Phys.* **2004**, *6*, 2224. (g) Wang, Y.; Liu, J. Y.; Li, Z. S.; Wu, J. Y.; Wang, L.; Sun, C. C. *Chem. Phys.* **2005**, *314*, 329.

(56) Beukes, J. A.; D'Anna, B.; Bakken, V.; Nielsen, C. J. *Phys. Chem. Chem. Phys.* **2000**, *2*, 4049.

(57) The experimental reaction enthalpy, ΔH_{rxn} (298 K), was calculated from the experimental $\Delta_f H°$ (298 K) of $^{\bullet}Cl$ and HCl,[45] and the experimental $H-CH_2CHO$ bond dissociation energy from Cumming and Kebarle.[58] The experimental vibrationless reaction energy, ΔE_{exp}, was calculated from ΔH_{rxn} (298 K) by subtracting the scaled QCISD/6-31+G(d,p) thermal corrections and zero-point vibrational energies.[53]

(58) Cumming, J. B.; Kebarle, P. *J. Am. Chem. Soc.* **1977**, *99*, 5818.

(59) The experimental reaction enthalpy, ΔH_{rxn} (298 K), was calculated from the experimental $\Delta_f H°$ (298 K) of $^{\bullet}Cl$ and HCl,[45] CH_3CO_2H,[32] and $^{\bullet}CH_2CO_2H$.[60] The experimental vibrationless reaction energy, ΔE_{exp}, was calculated from ΔH_{rxn} (298 K) by subtracting the scaled QCISD/6-31+G(d,p) thermal corrections and zero-point vibrational energies.[53] The $\Delta_f H°$ (298 K) of $^{\bullet}CH_2CO_2H$ was obtained from a combination of experimental measurements and density functional calculations.[60]

(60) Lagoa, A. L. C.; Diogo, H. P.; Dias, M. P.; Minas da Piedade, M. E.; Amaral, L. M. P. F.; Ribeiro da Silva, M. A. V.; Martinho Simoes, J. A.; Guedes, R. C.; Costa Cabral, B. J.; Schwarz, K.; Epple, M. *Chem.—Eur. J.* **2001**, *7*, 483.

(61) Wenthold, P. G.; Squires, R. R. *J. Am. Chem. Soc.* **1994**, *116*, 11890.

(62) The experimental reaction enthalpy, ΔH_{rxn} (298 K), was calculated from the experimental $\Delta_f H°$ (298 K) of $^{\bullet}Cl$ and HCl,[45] CH_3CO_2H,[32] and $^{\bullet}CH_2CO_2^-$,[61] and the experimental proton affinity of $CH_3CO_2^-$.[32,61] The experimental vibrationless reaction energy, ΔE_{exp}, was calculated from ΔH_{rxn} (298 K) by subtracting the scaled QCISD/6-31+G(d,p) thermal corrections and zero-point vibrational energies.[53]

(63) Harmonic frequency analysis at UQCISD/6-31+G(d,p) reveals that the C_{2v} stationary point possesses one imaginary frequency, whose normal mode diplacement corresponds to torsion about the C−C bond. The UQCISD/6-31+G(d,p) global mimimum has an O−C−C−H dihedral angle of 18.2° and lies 0.3 kJ mol^{-1} below the C_{2v} saddle point. Reoptimization and subsequent harmonic frequency analysis at both lower and higher levels of theory, including UCCSD/6-31+G(d,p), suggests, however, that $^{\bullet}CH_2CO_2^-$ adopts a planar C_{2v} minimum.

(64) Rudic, S.; Murray, C.; Harvey, J. N.; Orr-Ewing, A. J. *Phys. Chem. Chem. Phys.* **2003**, *5*, 1205.

(65) The experimental reaction enthalpy, ΔH_{rxn} (298 K), was calculated from the experimental $\Delta_f H°$ (298 K) of $^{\bullet}Cl$ and HCl,[45] CH_3NH_2, and $^{\bullet}CH_2NH_2$.[51] The experimental vibrationless reaction energy, ΔE_{exp}, was calculated from ΔH_{rxn} (298 K) by subtracting the scaled QCISD/6-31+G(d,p) thermal corrections and zero-point vibrational energies.[53]

JP9029437